

Crustal structure and relocated earthquakes in the Puget Lowland, Washington, from high-resolution seismic tomography

T. M. Van Wagoner,¹ R. S. Crosson, K. C. Creager, G. Medema, and L. Preston

Department of Earth and Space Sciences, University of Washington, Seattle, Washington, USA

N. P. Symons

Sandia National Laboratories, Albuquerque, New Mexico, USA

T. M. Brocher

U.S. Geological Survey, Menlo Park, California, USA

Received 13 June 2001; revised 19 July 2002; accepted 21 August 2002; published 31 December 2002.

[1] The availability of regional earthquake data from the Pacific Northwest Seismograph Network (PNSN), together with active source data from the Seismic Hazards Investigation in Puget Sound (SHIPS) seismic experiments, has allowed us to construct a new high-resolution 3-D, P wave velocity model of the crust to a depth of about 30 km in the central Puget Lowland. In our method, earthquake hypocenters and velocity model are jointly coupled in a fully nonlinear tomographic inversion. Active source data constrain the upper 10–15 km of the model, and earthquakes constrain the deepest portion of the model. A number of sedimentary basins are imaged, including the previously unrecognized Muckleshoot basin, and the previously incompletely defined Possession and Sequim basins. Various features of the shallow crust are imaged in detail and their structural transitions to the mid and lower crust are revealed. These include the Tacoma basin and fault zone, the Seattle basin and fault zone, the Seattle and Port Ludlow velocity highs, the Port Townsend basin, the Kingston Arch, and the Crescent basement, which is arched beneath the Lowland from its surface exposure in the eastern Olympics. Strong lateral velocity gradients, consistent with the existence of previously inferred faults, are observed, bounding the southern Port Townsend basin, the western edge of the Seattle basin beneath Dabob Bay, and portions of the Port Ludlow velocity high and the Tacoma basin. Significant velocity gradients are not observed across the southern Whidbey Island fault, the Lofall fault, or along most of the inferred location of the Hood Canal fault. Using improved earthquake locations resulting from our inversion, we determined focal mechanisms for a number of the best recorded earthquakes in the data set, revealing a complex pattern of deformation dominated by general arc-parallel regional tectonic compression. Most earthquakes occur in the basement rocks inferred to be the lower Tertiary Crescent formation. The sedimentary basins and the eastern part of the Olympic subduction complex are largely devoid of earthquakes. Clear association of hypocenters and focal mechanisms with previously mapped or proposed faults is difficult; however, seismicity, structure, and focal mechanisms associated with the Seattle fault zone suggest a possible high-angle mode of deformation with the north side up. We suggest that this deformation may be driven by isostatic readjustment of the Seattle basin. *INDEX TERMS:*

7205 Seismology: Continental crust (1242); 7218 Seismology: Lithosphere and upper mantle; 7230 Seismology: Seismicity and seismotectonics; *KEYWORDS:* tomography, structure, Puget, earthquakes

Citation: Van Wagoner, T. M., R. S. Crosson, K. C. Creager, G. Medema, L. Preston, N. P. Symons, and T. M. Brocher, Crustal structure and relocated earthquakes in the Puget Lowland, Washington, from high-resolution seismic tomography, *J. Geophys. Res.*, 107(B12), 2381, doi:10.1029/2001JB000710, 2002.

¹Now at ChevronTexaco North America Upstream, New Orleans, Louisiana, USA.

1. Introduction

[2] Although most damaging historical earthquakes in the region have been within the Wadati-Benioff zone of the Cascadia subduction zone (e.g., the 2001 magnitude 6.8 Nisqually earthquake [Malone *et al.*, 2001]), much

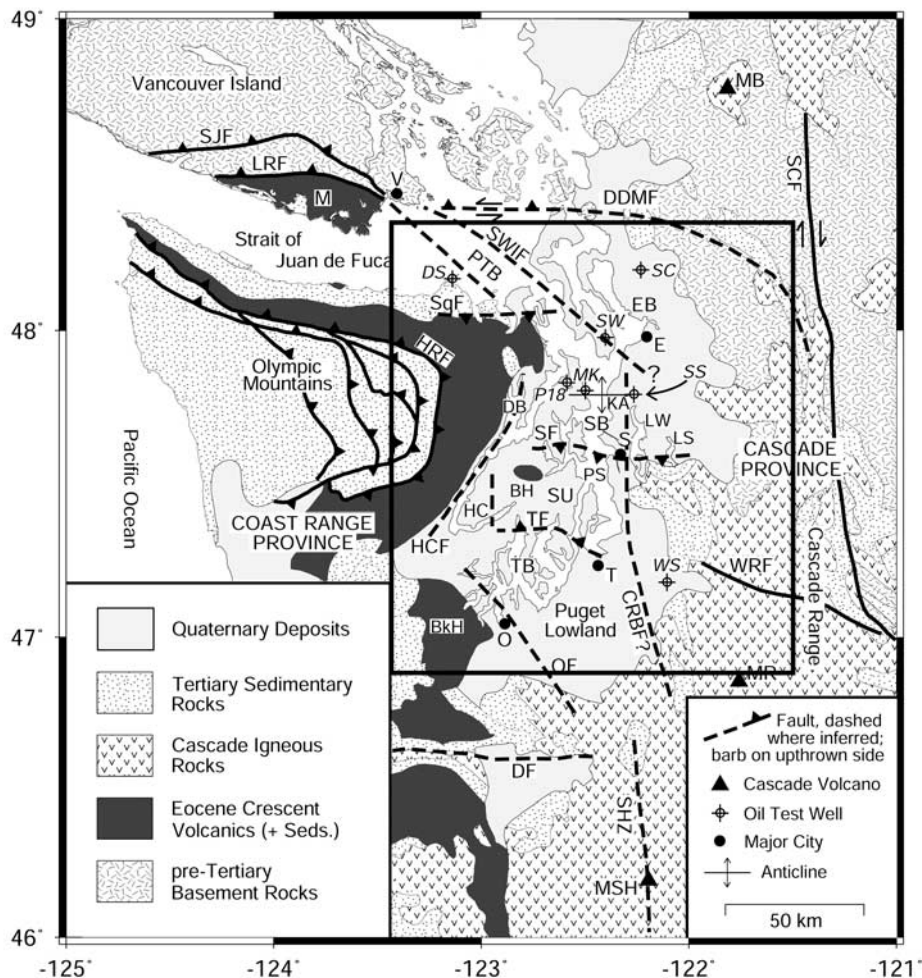


Figure 1. Schematic geologic map of northwestern Washington and southern British Columbia, showing the model region (heavy inner rectangle). Abbreviations for major cities: E—Everett; O—Olympia; S—Seattle; T—Tacoma; V—Victoria. Abbreviations for faults: CRBF—Coast Range boundary fault; DF—Doty fault; DDMF—Darrington—Devils Mountain fault; HCF—Hood Canal fault; HRF—Hurricane Ridge fault; LRF—Leech River fault; OF—Olympia fault; SCF—Straight Creek fault; SF—Seattle fault; SHZ—St. Helens zone; SJF—San Juan fault; SqF—Sequim fault; SWIF—Southern Whidbey Island fault; TF—Tacoma fault; WRF—White River fault. Abbreviations for oil test wells: DS—Dungeness Spit #1; MK—Mobil Kingston #1; P18—Pope-Talbot #18-1; SC—Silvana Community #12-1; SS—Social Schroeder #1; SW—Social Whidbey #1; WS—Washington State #1. Abbreviations for geologic, structural, and topographic features: BH—Blue Hills; BkH—Black Hills; DB—Dabob Bay; EB—Everett basin; HC—Hood Canal; KA—Kingston arch; LS—Lake Sammamish; LW—Lake Washington; M—Metchosin igneous complex; PTB—Port Townsend basin; PS—Puget Sound; SB—Seattle basin; SU—Seattle uplift; TB—Tacoma basin. Abbreviations for Cascade volcanoes: MSH—Mt. St. Helens; MR—Mt. Rainier; MB—Mt. Baker. Sources: *Blakely et al.* [2002]; *Brocher et al.* [2001]; *Brocher and Ruebel* [1998]; *Gower et al.* [1985]; *Johnson et al.* [1999]; *Schruben et al.* [1994]; *Tabor and Cady* [1978a].

recent geological and geophysical research in the Puget Lowland of western Washington State (Figure 1) has been prompted by increasing concern about hazards from crustal earthquake sources. A postulated earthquake about 1100 years ago on the Seattle fault [*Bucknam et al.*, 1992] and concern about other possible crustal faults [e.g., *Johnson et al.*, 1996, 1999] in the Lowland region motivated the recent SHIPS active source experiments [*Brocher et al.*, 1999, 2000], and analyses based on these and other

investigations [e.g., *Brocher et al.*, 2001; *Blakely et al.*, 2002].

[3] *Lees and Crosson* [1990] carried out the first 3-D tomography for the Puget Lowland region, but were limited by relatively few earthquake observations and sparse station spacing. *Symons and Crosson* [1997] developed new inversion technology and applied this to an improved earthquake data set plus limited explosion data. In their study, shallow resolution was again limited by lack of surface source to

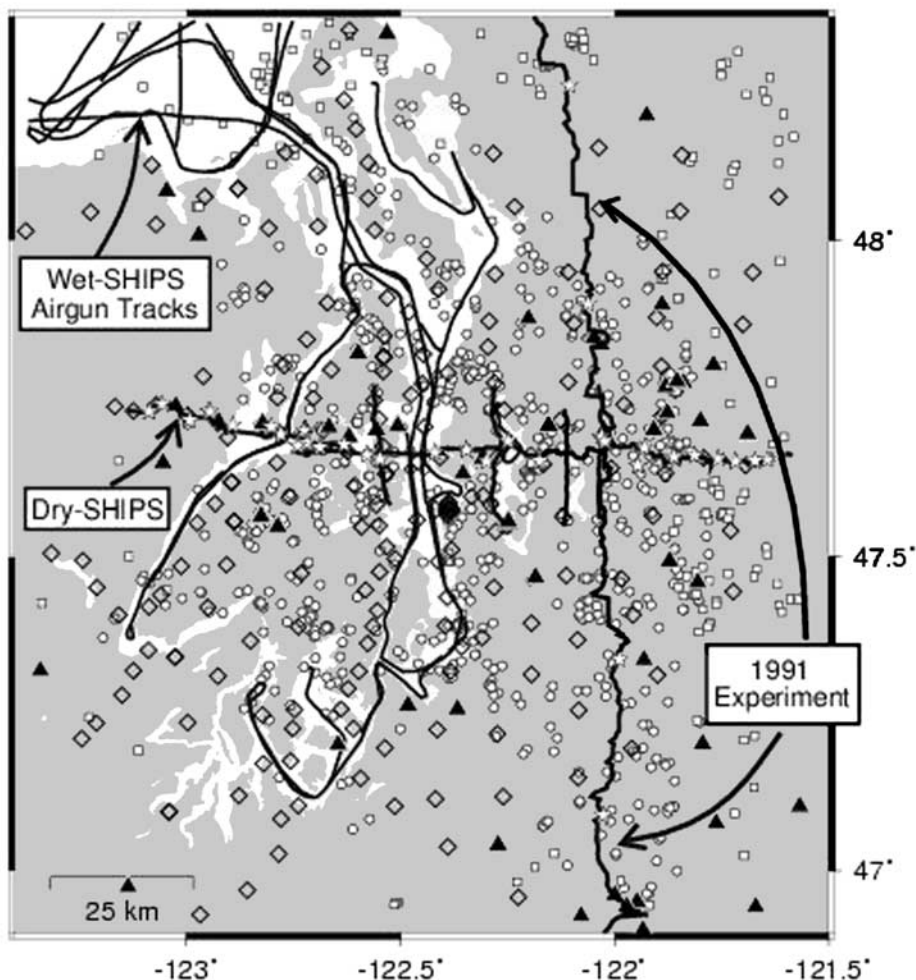


Figure 2. Map of the Puget Lowland model area showing source/receiver locations used to construct the high resolution model. The map area is the heavy inner rectangle shown in Figure 1. Temporary Wet-SHIPS stations are shown as diamonds (\diamond) and Wet-SHIPS air gun tracks are shown as thin line segments. Permanent PNSN seismograph stations are shown as black triangles. Station distributions for both the Dry-SHIPS and the 1991 experiment are shown as line segments and experimental sources are shown as white stars. Higher confidence 3-D relocated earthquake epicenters are shown as white circles (\circ), lower confidence events as white squares (\square). Earthquake observations were recorded only by PNSN stations.

surface receiver observations. Seismic reflection profiling has been interpreted for structural details in only the upper few kilometers at most of the crust [e.g., *Johnson et al.*, 1994, 1996; *Pratt et al.*, 1997]. More recently, a first arrival P wave tomography model for the upper 11 km of the crust was constructed by *Brocher et al.* [2001] in the same region as our study using data from the initial SHIPS experiment. In these previous studies, the structural transition to mid-crustal depths has not been accurately imaged. Since the midcrust is likely to be the seat of important tectonic processes in this forearc region, potentially valuable structural information has been missing.

[4] The availability of active source data from SHIPS as well as two earlier experiments [*Miller et al.*, 1997; *Parsons et al.*, 1999], together with high quality crustal earthquake data acquired for the last 20 years from the PNSN regional network (Figure 2), provides an ideal opportunity to refine

our knowledge of the crustal structure in this region. In this study, the simultaneous analysis of earthquake data and active source observations has allowed us to develop a high quality 3-D model to a depth of 30 km, considerably greater than previously reported [e.g., *Brocher et al.*, 2001], and to simultaneously relocate nearly 1000 regional earthquakes for tectonic interpretation.

1.1. Geologic Setting

[5] The tectonics of the Pacific Northwest region are dominated by the oblique, northeastward subduction of the Juan de Fuca plate beneath western North America. Subduction of oceanic lithosphere during the Tertiary has led to the formation of two major geologic provinces in the region: the Coast Range province on the west, which includes the Olympic subduction complex (OSC) plus the Puget Lowland, and the Cascade province on the east

(Figure 1) [Brandon and Calderwood, 1990; Snively and Wells, 1996].

[6] In the OSC, metamorphosed Tertiary sedimentary rocks from the accretionary prism have been uplifted since the Miocene to form the Olympic mountains [Tabor and Cady, 1978a; Brandon et al., 1998]. Within the eastern Olympics is the steeply dipping Crescent Formation—thick submarine and subaerial Paleocene to Eocene basalts which may have formed by extrusion associated with extension along the margin of north America [Wells et al., 1984; Babcock et al., 1992]. Olympic uplift has tilted the Crescent to its present east-dipping position on the western boundary of the Lowland [Tabor and Cady, 1978a, 1978b; Brandon and Calderwood, 1990]. The Crescent formation is correlated with the Siletz River volcanics in Oregon [Snively and Baldwin, 1948], the Metchosis igneous complex on southern Vancouver Island [Massey, 1986], and with basalt outcrops in the Blue Hills east of Bremerton and in the Black Hills southwest of Olympia (Figure 1) [Babcock et al., 1994]. Thickness of the Siletz volcanics in Oregon may be as much as 34 km [Trehu et al., 1994], possibly thinning northward into Washington where mapped thickness of the Crescent is more than 16 km [Babcock et al., 1992] and tomographic imaging reveals Crescent extending to depths as great as 25 km [Symons and Crosson, 1997].

[7] The eastern boundary of the Coast Range province is ill-defined beneath the Puget Lowland where it contacts the pre-Tertiary basement of the Cascade province. The Cascade basement comprises a variety of igneous, metamorphic, and sedimentary rocks which were accreted to North America by the late Cretaceous or early Tertiary [Tabor, 1994]. Cascade arc volcanism began in the late Eocene [Snively and Wells, 1996].

1.2. Seismicity

[8] Earthquakes in western Washington generally fall into two categories: crustal events which occur at depths less than about 30 km, and subcrustal events associated with the subducted oceanic lithosphere which typically occur at depths greater than 35 km [Ludwin et al., 1991]. The majority of crustal earthquakes in western Washington occur beneath the Puget Lowland and the eastern edge of the Cascade volcanic arc, with virtually none occurring in the OSC. The largest crustal earthquakes with modern network observations in the Puget Lowland are the magnitude 5.0 Robinson Point event in 1995, the magnitude 5.4 Duvall event in 1996, and the magnitude 4.9 Bremerton earthquake in 1997. A probable crustal earthquake with an estimated magnitude greater than 6.5 occurred in 1872 to the northeast of the study area in the North Cascades [Malone and Bor, 1979; Bakun et al., 2001]. Focal mechanisms for crustal earthquakes beneath the Puget Lowland are mainly thrust and strike-slip, with shallowly plunging P-axes oriented north-south [Ludwin et al., 1991; Ma et al., 1996].

1.3. Shallow Structure and Faulting

[9] The shallow structure of the Puget Lowland consists of sedimentary basins and relative basement highs delineated mainly by gravity and seismic reflection observations. Pratt et al. [1997] interpreted these structures to have formed in a compressive tectonic regime. The identi-

fication of faults with possible reverse offsets [e.g., Johnson et al., 1994, 1999; Brocher et al., 2001] is consistent with the focal mechanisms of crustal earthquakes [Ma et al., 1996]. Northward compression is most likely the result of oblique subduction [Wang, 1996], possibly in conjunction with northward migration of the Cascadia forearc [Brandon and Calderwood, 1990; Wells et al., 1998].

[10] Geologic identification of shallow faults is hampered by thick glacial sediments covering much of the Lowland and diffuse crustal seismicity does not reveal distinct lineations that may be interpreted as active faults. Various geophysical techniques, including gravity and magnetic surveys, seismic reflection profiles, and seismic tomography, have been employed to identify faults and other structures [e.g., Danes et al., 1965; Blakely et al., 1999; Pratt et al., 1997; Brocher et al., 2001].

[11] The most important shallow fault zone in the region is the E-W striking Seattle fault which runs directly beneath the Seattle metropolitan area and has been interpreted to be a south-dipping thrust or reverse fault (Figure 1) [Johnson et al., 1994, 1999; Pratt et al., 1997]. The Seattle fault forms the southern boundary of the Seattle basin, an approximately 10 km deep basin composed of low velocity, low density sedimentary rocks with a negative Bouguer gravity anomaly exceeding -120 mGal [Danes et al., 1965; Finn et al., 1991; Johnson et al., 1994]. The upper 10–12 km of the crust within the Seattle fault zone have been imaged by recent seismic reflection surveys and may consist of multiple E-W oriented fault segments [Fisher et al., 1999; Molzer et al., 1999; ten Brink et al., 2002]. South of the Seattle fault, Crescent basement lies close to the surface [e.g., Pratt et al., 1997]. Reverse displacement on the Seattle fault has been interpreted to be responsible for both uplift of the basement south of the fault and subsidence of the Seattle basin north of the fault [Johnson et al., 1994, 1999; Pratt et al., 1997].

[12] Paleoseismic investigations revealed an uplifted marine terrace at Restoration Point on Bainbridge Island which suggests an earthquake, possibly of magnitude 7.0 or greater, occurred on the Seattle fault approximately 1100 years ago [Bucknam et al., 1992]. Also within the Seattle fault zone is a recently discovered north-dipping fault scarp on southern Bainbridge Island with evidence of north-side-up offset within the last 3–4 ka [Bucknam et al., 1999; Nelson et al., 1999].

[13] South of the Seattle fault zone, a bounding fault on the north side of the Tacoma basin was proposed by Danes et al. [1965] from gravity data, and by Gower et al. [1985] based on gravity and aeromagnetic anomalies. Velocity gradients from shallow tomography, in addition to documented uplift at two localities north of the Tacoma basin [Bucknam et al., 1992; Sherrod, 1998], led Brocher et al. [2001] to interpret this boundary as a north-dipping reverse fault, designated the Tacoma fault.

[14] Northward motion of the Cascadia forearc region during the early Tertiary may have been accommodated along the proposed Coast Range Boundary fault (CRBF), a right-lateral strike-slip fault which presumably separates rocks of the Coast Range terrane from the pre-Tertiary basement of the Cascades [Johnson, 1984, 1985; Johnson et al., 1996]. The CRBF is inferred mainly from sedimentologic evidence to lie beneath the eastern Puget Lowland

where it strikes approximately N–S (Figure 1). As a possible extension of the CRBF, the northern boundary between the Coast Range basement and the Cascade block is the southern Whidbey Island fault zone, a NW trending transpressional fault [Johnson *et al.*, 1996], which may in turn connect with the Leech River fault to the west on southern Vancouver Island where the terrane boundary is exposed at the surface (Figure 1) [Clowes *et al.*, 1987; Johnson *et al.*, 1996].

2. Data Description

[15] Data used to construct our model originated from three active source seismic experiments, and from earthquakes recorded by the permanent Pacific Northwest Seismograph Network (PNSN) operated by the University of Washington (Figure 2).

2.1. Active Source Data

[16] Counting the number of source-receiver P wave arrivals, eighty-one percent of the data originated from the first phase of the Seismic Hazards Investigation of Puget Sound (SHIPS), nicknamed “Wet-SHIPS”, during which approximately 250 temporary land-based seismographs were deployed to record more than 33,000 air gun sources in the waterways of Puget Sound and the Straits of Juan de Fuca and Georgia (Figure 2) [Brocher *et al.*, 1999]. Nearly one million travel time picks from the Wet-SHIPS project were initially made by USGS and other project collaborators [Brocher *et al.*, 2001]. In order to minimize redundancy in the data and for computational efficiency, we divided our model area into 0.7 km^2 grids and then selected one source in each grid element that had the largest number of associated picks, resulting in a total of 64,675 first-arrival picks which were used in our inversion.

[17] The second phase of the SHIPS project was an E–W land refraction experiment, nicknamed “Dry-SHIPS”, during which more than 1000 temporary land-based seismographs were deployed across the central Puget Lowland to record 38 drill hole sources (Figure 2) [Brocher *et al.*, 2000]. From the trace data we made 3588 first-arrival picks from 32 shots, all of which were included in the inversion, representing 4.5% of the total data. Also included in the inversion were 880 travel times from 5 land sources recorded by 252 temporary land-based seismometers deployed during the 1991 N–S land refraction experiment (Figure 2) on the west flank of the Cascade Range [Miller *et al.*, 1997], and 39 travel times from three of these sources recorded by permanent PNSN stations. For all active source data, water depth time corrections were applied and picking error is assumed to be 50 ms.

2.2. Earthquake Data

[18] A total of 912 earthquakes, selected from the PNSN catalog from 1980 through 2000, was used in the inversion (Figure 2). Events prior to 1980 were not digitally recorded and were not included in the inversion because of difficulty in verifying timing. Two earthquake databases were constructed with different selection criteria. The first group of earthquakes are the highest quality and possess at least one of the following three characteristics: (1) magnitude greater than or equal to 2.5, or (2) at least 10 P wave arrival picks,

maximum RMS residual of 0.3 s, maximum estimated errors in the hypocenter location of 2.5 km horizontally and 5.0 km vertically, maximum azimuthal gap of 135° , and maximum distance to the nearest station of less than twice the event depth (or 10 km, whichever is greater), or (3) more than 20 P-picks [Symons, 1998]. The high quality earthquakes were declustered to remove redundancy and repicked to ensure accuracy, resulting in 555 events. The second group of earthquakes are medium quality and consist of 357 events with the following characteristics: (1) magnitude greater than or equal to 2.0, and (2) at least 10 picks of the P wave arrival, and (3) maximum azimuthal gap of 160° . Events in the medium quality database were also repicked to ensure accuracy.

3. Tomography Method and Results

[19] P wave first-arrival observations from both earthquakes and explosions were used to generate a P wave velocity model of the Puget Lowland. The model is defined within a rectangular box between longitudes 123.4°W and 121.5°W , latitudes 46.9°N and 48.35°N , and extending from above the surface to 40 km depth (Figure 2). Model coordinates are given throughout the paper in kilometers east (E) and north (N) from 46.9°N and 123.4°W . For convenience, these are given in the text as coordinate pairs in parentheses—for example: (80, 95), where the position is 80 km east and 95 km north. Single coordinate values are stated as kilometers east or north (e.g., 80 E or 40 N). The velocity model is defined on a grid of nodes within the model space, with a node spacing of 1.5 km in both horizontal and vertical dimensions, resulting in 331,360 total velocity model parameters.

[20] Nonlinear 3-D seismic tomography was carried out by the method of Symons and Crosson [1997], which jointly inverts arrival time observations from both earthquakes and explosions to simultaneously obtain a P wave slowness (inverse of velocity) model and relocated earthquake hypocenters. The method is fully nonlinear, using linearized iterations to achieve a minimum L2 norm between observations and theoretical predictions. Travel times are computed by finite difference using nodal parameterization. Each constraint equation in the linearized system is weighted by the inverse of its picking error, with regularization imposed to smooth the final model. We utilized a discrete Laplacian regularization operator which uses the six nearest neighbors on the rectangular grid of nodes. This operator is anisotropic with a horizontal to vertical smoothing ratio of 5. The linearized system is solved at each iteration by conjugate gradient least squares. The model and hypocenters are updated after each iteration and the inversion is repeated until the norm of the model perturbation falls below a small predetermined value, typically in less than 20 iterations. Since our model is fully three-dimensional, separate station corrections, which are commonly used to approximate lateral velocity variations near stations, are not necessary and were not included in the model parameterization.

[21] Initial earthquake hypocenters used in the inversion were determined using the current PNSN Puget Sound velocity model and station corrections [Crosson, 1976; Ludwin *et al.*, 1991]. A slightly modified version of the

Table 1. 1-D Starting Model

Depth Range, km	P-Velocity, km/s
0.0–1.0	4.00
1.0–5.0	5.80
5.0–10.0	6.60
10.0–15.0	6.75
15.0–20.0	6.85
20.0–25.0	6.95
25.0–40.0	7.80

PNSN 1-D model, based on preliminary inversion trials, was used as our starting model for the 3-D inversion (Table 1).

[22] Several regularization weights were tried in order to generate models with varying degrees of smoothness. Our preferred final model, designated PS3DA, had small overall travel time residuals and is realistic compared to previous models and to current knowledge of geologic structure beneath the Lowland. Models with larger regularization weights had unreasonably large residuals and models with smaller weights were unrealistically rough. The overall RMS residual for the best fitting 1-D model is 710 ms, while that

for model PS3DA is 97 ms—this represents a simple residual variance reduction of 98%.

3.1. Resolution

[23] To determine the resolving ability of our model, we performed a series of 3-D checkerboard tests in which model PS3DA was perturbed by adding a 3-D sinusoidal pattern with a maximum amplitude of 10% of the model velocity value (maximum of ± 0.81 km/s). The sinusoid wavelength is variable for different tests (Figure 3). Synthetic travel times were then generated through the perturbed model using the same source-receiver positions as for the actual data. Using the smoothing parameters from our final model, we inverted the synthetic travel times, allowing the hypocenters to be simultaneously relocated. The vertical sinusoid wavelength was fixed at 20 km, producing a vertical cell size of 10 km. Two separate inversions using both 20 km and 30 km horizontal wavelengths were performed, resulting in 10 and 15 km grids in map view.

[24] The checkerboard pattern has been recovered remarkably well at both the 15 and 10 km cell spacing (Figure 3).

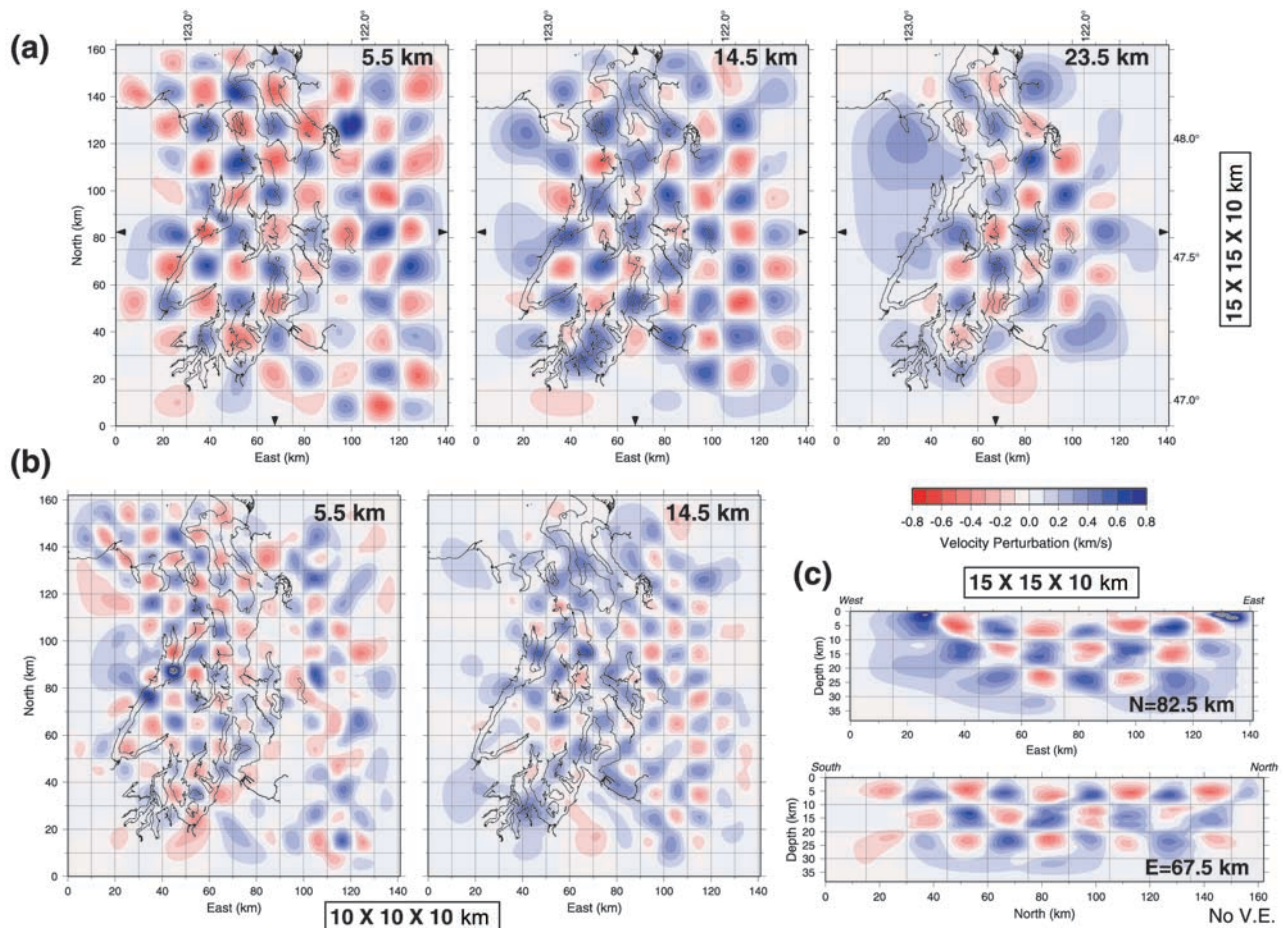


Figure 3. Recovered sinusoidal checkerboard perturbations from the final 3-D model using a vertical cell spacing of 10 km. (a) Horizontal slices with a lateral anomaly spacing of 15 km, (b) horizontal slices with a lateral anomaly spacing of 10 km, and (c) vertical sections through the 15 km lateral anomaly perturbation whose locations are shown by black pointers in (a). Grid lines show boundaries of original checkerboard pattern. Grid dimensions listed in black boxes are kilometers east, north, and depth respectively.

The model is best resolved laterally in the upper 10 km due largely to the active source constraint. At 5.5 km depth the 15 km cell pattern and the perturbation amplitudes have been recovered well throughout the majority of the model (Figures 3a and 3c). At this depth, cell spacing of 10 km has also been recovered well with some loss of resolution on the western and southern edges and north and south of Lake Washington where ray coverage is minimal (Figure 3b).

[25] At 14.5 km depth, the 15 km cell spacing has been recovered throughout most of the model area and the majority of the 10 km cell spacing in the central and eastern parts of the model has also been recovered (Figures 3a and 3b). Observations at this depth and below originate mostly from earthquake sources, as most ray paths from the active source surveys do not penetrate to this depth. Smearing of velocities between adjacent cells at the 10 km spacing and no recovered checkerboard pattern beneath the western part of the model area at 14.5 km depth reveals little to no resolution in these regions (Figure 3b). At 23.5 km depth, the 15 km cell spacing in the central portion of the model has been recovered where earthquakes are located (Figure 3a).

[26] Vertical anomalies of 10 km are recovered well throughout the upper 30 km of the model (Figure 3c) where the recovered checkerboard pattern reveals a concave-upward zone which closely parallels the distribution of earthquake hypocenters. Perturbations in the upper 2–5 km of the model are not fully recovered due to ray coverage that is primarily focused around stations. Two anomalous, high velocity regions are observed in E–W cross-section (Figure 3c) in the upper few kilometers due to overshoot effects near the model edges where observational constraints are lacking. The model is poorly resolved deeper than 30 km due to the sparse occurrence of earthquakes below that depth.

3.2. Comparisons

3.2.1. Borehole Sonic Data and Laboratory Velocities

[27] Since direct verification of tomography models is difficult, we compared model PS3DA with measured sonic velocity logs from six oil exploration wells in the Puget Lowland whose locations are shown in Figure 1 [Brocher and Ruebel, 1998]. Based on this comparison, model PS3DA velocities closely match the mean measured sonic speeds within the upper 2–3 km of the crust for the few sites in the central portion of the model.

[28] The top of the Crescent formation is encountered in the Dungeness Spit, the Mobil Kingston #1, and the Pope Talbot #18-1 wells at approximately 1.5, 2.2 and 1 km depth, respectively. Sonic speeds increase by 50–60% to 4.0–6.0 km/s where the basalt is reached. At the depths of this contact, PS3DA velocities are averages of the shallow low velocity rocks and the higher velocity basalt, yielding velocities in the range of 3.5–5.0 km/s. Measured sonic speeds in the Kingston well are unavailable at the depth of the contact, but our model velocities are between 3.5 and 4.0 km/s. Although these wave speeds slightly underestimate the likely velocity of the basalt, model PS3DA velocities increase sharply below this depth to exceed 4.5 km/s at 3.5 km depth.

[29] In general, the Crescent basement is deeper than 2 km and we expect its velocity to exceed 4.5 km/s. Mean P

Table 2. Laboratory P Wave Velocities for Western WA “Mafic Rocks”^a

Pressure, MPa	Approximate Depth, km	Average P-Velocity, km/s
20	0.7	5.82 ± 0.51
40	1.5	5.93 ± 0.46
60	2.2	5.99 ± 0.42
80	2.9	6.04 ± 0.41
100	3.6	6.07 ± 0.40
200	7.3	6.18 ± 0.36

^aVelocities are reported as averages and standard deviations of measurements at each respective pressure [Brocher and Christensen, 2001].

wave velocities of 29 Crescent formation rocks collected from the Olympic Peninsula and the Blue Hills increase on average from 5.8 to 6.2 km/s over confining pressures corresponding to depths of about 0.7–7.3 km (Table 2) [Brocher and Christensen, 2001]. The standard deviations of these velocities are about 10% of the means. These values are consistent with published measurements from global samples of unaltered basalts, while velocities for zeolite to prehnite-pumpellyite facies basalt vary from 6.2 to 6.4 km/s over the same temperature and pressure range [Christensen and Mooney, 1995]. Although Crescent basalts contain zeolite and prehnite-pumpellyite alteration minerals, this formation also includes basaltic conglomerate and interbedded marine sedimentary units [Taber and Cady, 1978a] which reduce its expected P wave velocity. Based on these laboratory and borehole observations, we expect the Crescent formation to have velocities of 4.5–5.5 km/s at depths less than 5 km, and velocities of 5.5–6.5 km/s at depths greater than 5 km. Sonic speeds of sedimentary and some volcanoclastic rocks in these exploration wells typically range from 1.5 to 4.5 km/s; we thus interpret model velocities less than 4.5 km/s to represent sedimentary rocks.

3.2.2. Refraction Profiles

[30] The profile analyzed by Schultz and Crosson [1996] slants across the southern portion of our model and is roughly comparable to Figure 4a. Although the resolution of this profile cannot approach the 3-D tomography resolution, velocities at 10–15 km depth are comparable at approximately 6.5 km/s indicating good average agreement. The N–S profile along the Cascade range front analyzed by Miller *et al.* [1997] lies about 15 km east of the section shown in our Figure 5c. Velocity gradients and values are in generally good agreement between this profile and our model in the upper 20 km of the crust; however, the Muckleshoot basin, which is readily apparent on our cross-section, is not apparent on the Miller *et al.* [1997] profile, probably because their profile lies almost entirely east of the basin.

4. Interpretation and Discussion

4.1. Velocity Model

[31] Our final P wave velocity model (PS3DA) is illustrated in a series of color maps and cross-sections (Figures 4–6, including computed earthquake locations, with color scales to represent velocity intervals. In this subsection we describe important features of the velocity model and our

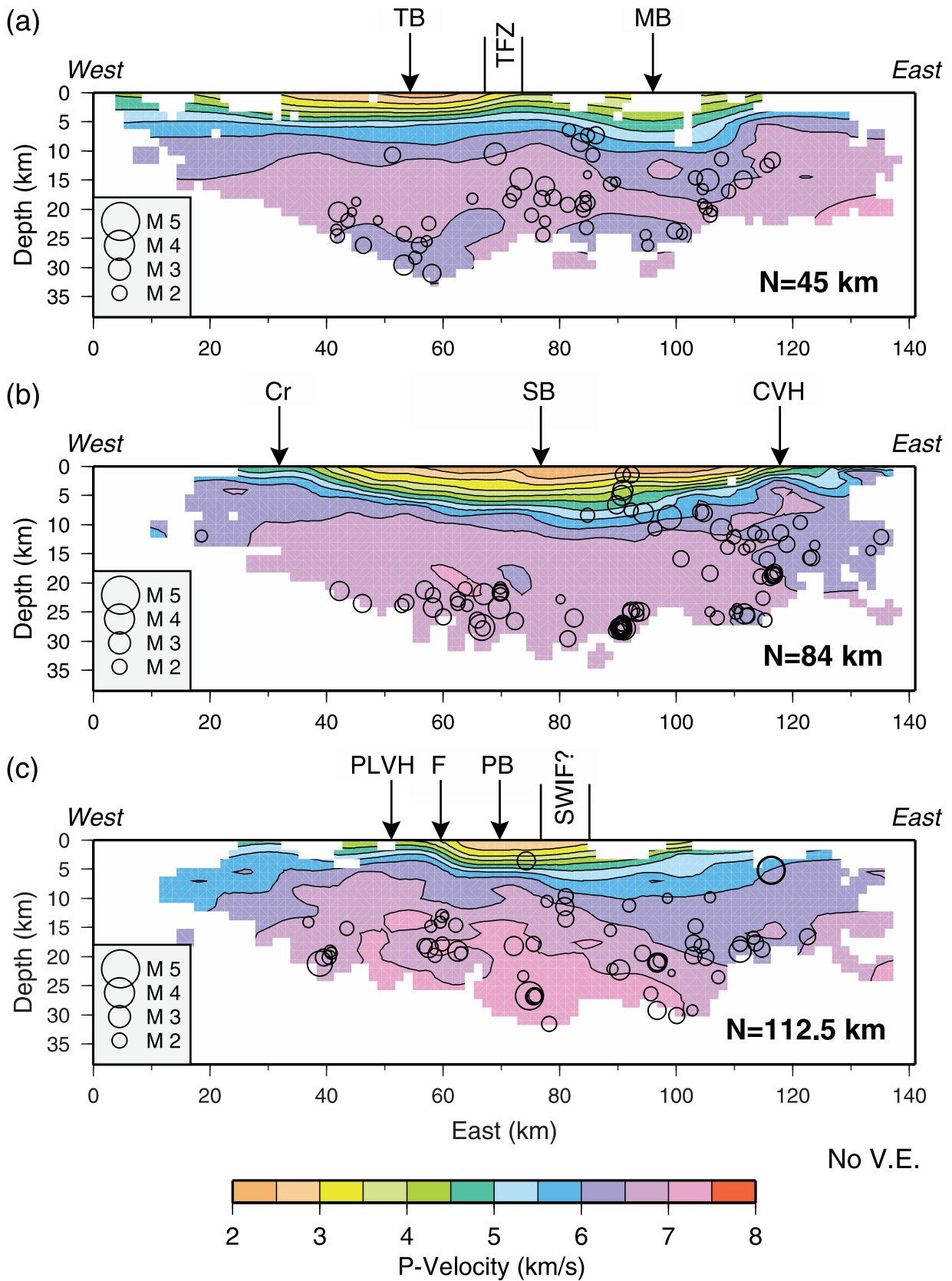


Figure 4. East–West cross-sections through the velocity model showing 3-D earthquake hypocenters within ± 5 km of respective vertical section. Coordinates of cross-section locations are noted in lower right corner and shown in Figure 6 as red pointers. Structural abbreviations: CVH—Carnation velocity high; Cr—Crescent Fm (at surface); F—unnamed fault. Remaining structural abbreviations defined in Figure 5. Earthquake magnitude scale shown in the lower left corner.

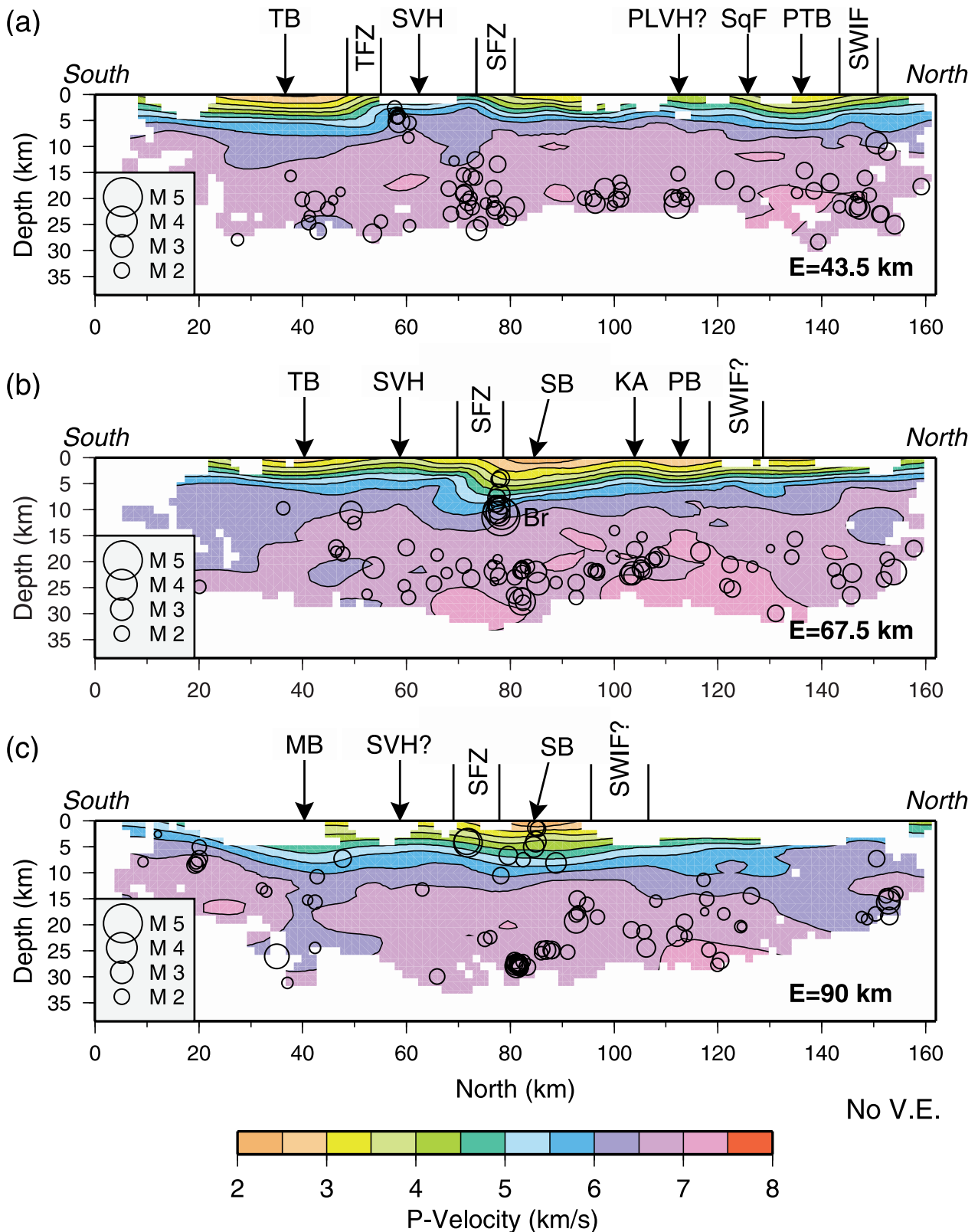


Figure 5. North–South cross-sections through the velocity model showing 3-D earthquake hypocenters within ± 5 km of each respective vertical section. Coordinates of cross-section locations are noted in lower right corner and shown in Figure 6 as red pointers. Structural abbreviations: KA—Kingston arch; MB—Muckleshoot basin; PB—Possession basin; PLVH—Port Ludlow velocity high; PTB—Port Townsend basin; SB—Seattle basin; SFZ—Seattle fault zone; SqF—Sequim fault; SVH—Seattle velocity high; SWIF—Southern Whidbey Island fault zone; TFZ—Tacoma fault zone; TB—Tacoma basin. Earthquake magnitude scale shown in the lower left corner.

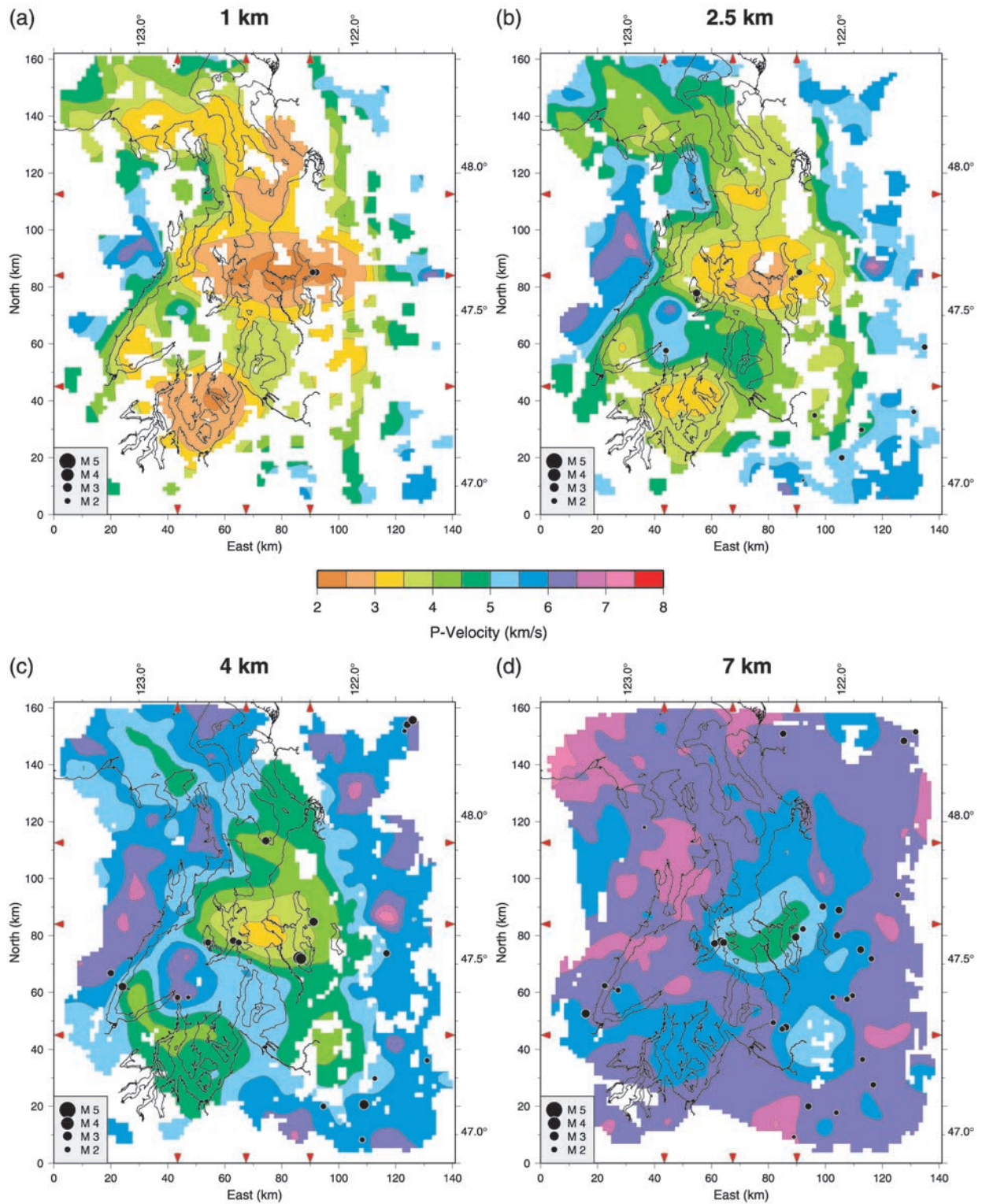


Figure 6. Horizontal depth slices through the 3-D model showing P wave velocities and 3-D earthquake hypocenters within ± 1 km of each respective horizontal section. Model coordinates are measured in kilometers North and East from 123.4° W longitude and 46.9° N latitude. Velocities in regions of the model unconstrained by observations are not plotted. Red pointers show locations of cross-sections shown in Figures 4 and 5. Earthquake magnitude scale is shown in the lower left corner. Note the different velocity scale for e–h.

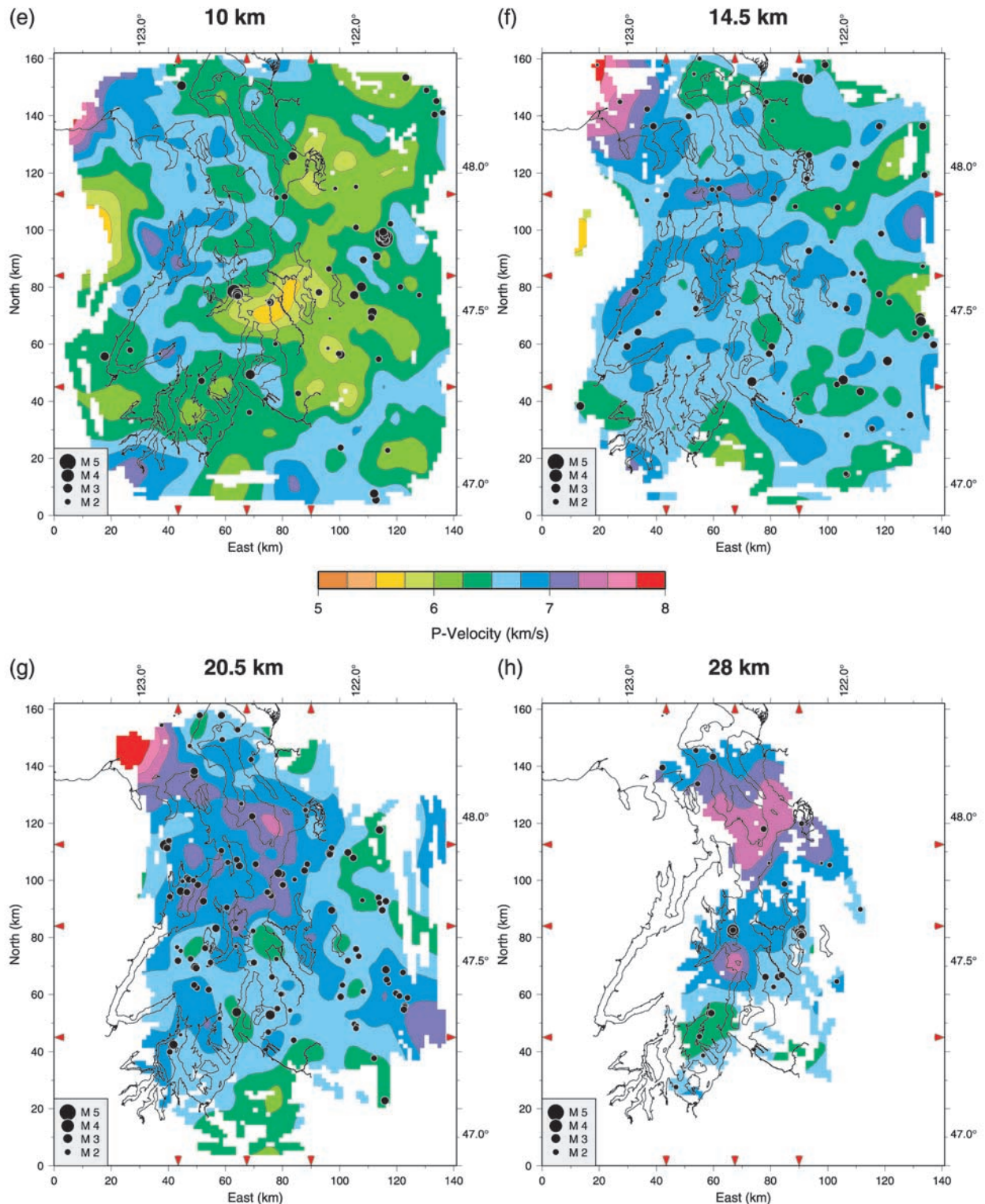


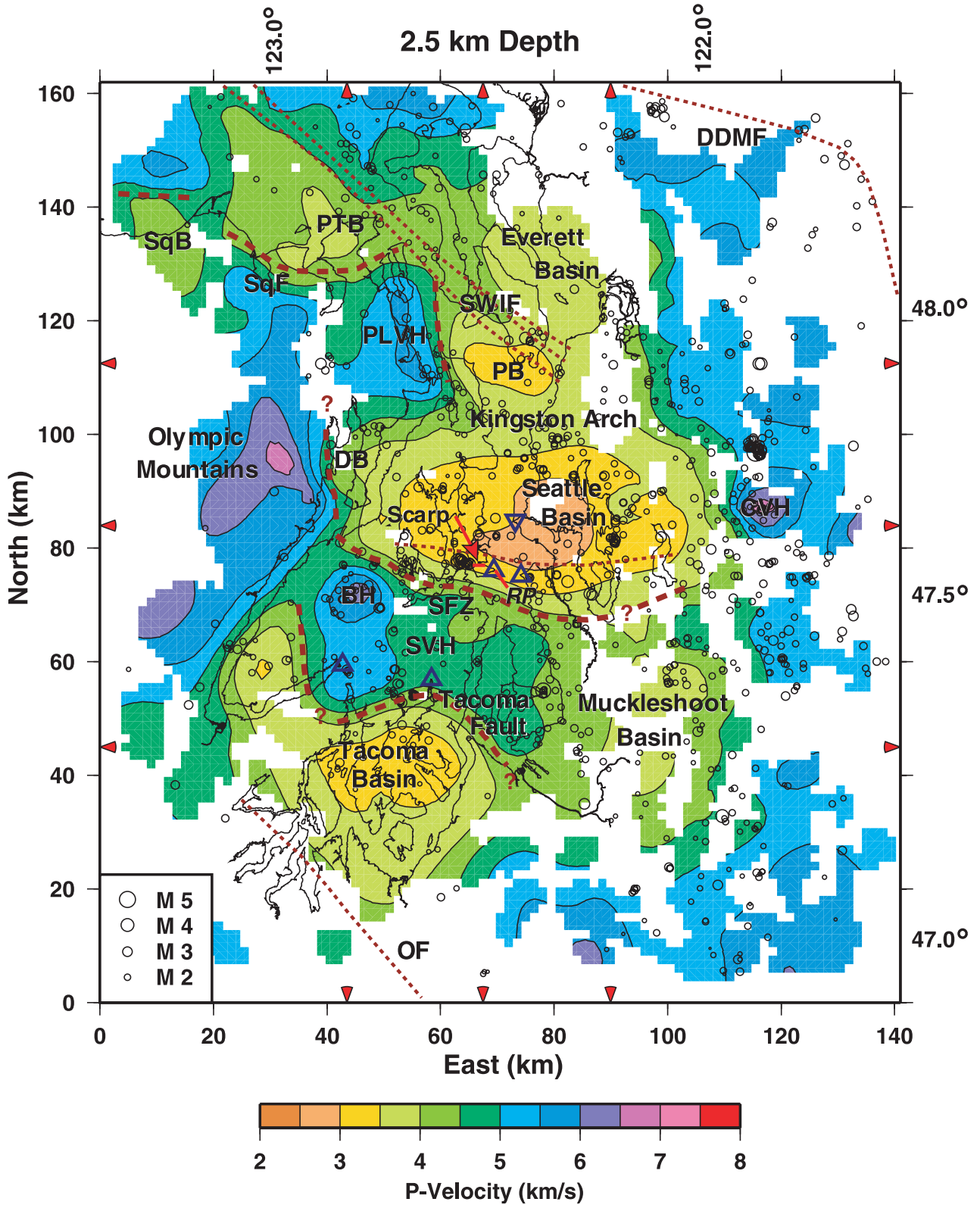
Figure 6. (continued)

interpretation of significant structure as summarized in Figure 7.

4.1.1. Tacoma Basin and Fault

[32] The Tacoma basin, near model coordinates (50, 40), is characterized by a negative Bouguer gravity anomaly

which is multilobed and elongated NW [Finn *et al.*, 1991]. The Tacoma basin can be divided into two regions—one portion approximately 25 by 35 km underlying south Puget Sound, and a NW trending linear segment approximately 15 by 30 km underlying the southern portion of Hood Canal



(Figures 6a, 6b, and 6c). In N–S cross-section, the main segment of the basin is asymmetric, with low velocity rocks deeper to the north (Figure 5a). The thickness of sedimentary units in the Tacoma basin was estimated to be 3.5 km by *Pratt et al.* [1997] based on seismic reflection profiles. The basin reaches depths of 5–7 km (5.5 km/s velocity contour, Figures 4a and 5a) in our model and is truncated to the north by steep velocity gradients (Figure 5a, 55 N) which we interpret to be a fault due to its coincidence with sharp gravity and magnetic anomalies [*Danes et al.*, 1965; *Finn et al.*, 1991; *Blakely et al.*, 1999]. It was identified as a fault by *Danes et al.* [1965] and designated the Tacoma fault by *Brocher et al.* [2001]. Vertical offset on the Tacoma fault appears to be several kilometers, but the dip of the fault cannot be confidently resolved by tomography. We have also imaged the eastern boundary of the north-trending, narrow-lobed portion of the basin (Figures 6a–6c, coordinates (30, 60)). The sharp velocity gradient along this boundary may represent a northward continuation of the Tacoma fault as suggested by *Brocher et al.* [2001].

4.1.2. Seattle Velocity High (SVH)

[33] The SVH is a NW trending block of high velocity rock at relatively shallow depth (1–3 km) that separates the Seattle and Tacoma basins (Figures 6a–6c, coordinates (60, 60)). This structural unit is called the “Seattle uplift” by several authors [e.g., *Pratt et al.*, 1997] and interpreted as elevated Crescent basement with exposures of Crescent on the west side of the unit in the Blue Hills southwest of Bremerton (Figure 1) [*Yount and Gower*, 1991; *Haeussler and Clark*, 2000]. Since there is no direct evidence of major basement uplift in the SVH, we prefer the tectonically neutral name of velocity high rather than uplift for this feature. The maximum surface elevation of the SVH is 537 m at Gold Mountain and for most of the structural block, basement velocity is reached at 1–3 km depth. The Bouguer gravity over the SVH is close to zero [*Danes et al.*, 1965; *Finn et al.*, 1991] suggesting that this region, which is topographically near sea level, is close to isostatic equilibrium.

[34] The tomographic image of the SVH is a 50 by 25 km block with what appears to be a thin (1–2 km) sediment package overlying Crescent basement on the eastern portion, and limited surface exposure of Crescent on the western portion (Figures 5a and 5b). The southern boundary of the SVH is the proposed Tacoma fault, which separates high velocity basement rock from the lower velocity rocks of the Tacoma basin. The western portion of the SVH contains two subcircular high velocity features (Figure 6c, near coordinates (45, 60)), coincident with magnetic highs [*Blakely et al.*, 1999], the northern-most of which reaches the surface in the Blue Hills. The northwest corner of the SVH appears to be continuous with rocks west of Hood Canal at and below

4 km depth (Figures 6c and 6d), which we interpret to be the Crescent formation due to its similarly high velocity (5–6.5 km/s) and its traceable surface exposure west of Hood Canal. This relationship suggests direct structural connection between uplifted Crescent formation on the Olympic Peninsula and the Crescent rocks of the SVH.

4.1.3. Muckleshoot Basin

[35] Southeast of the SVH, near model coordinates (95, 45), is a previously undescribed basin approximately 20 by 25 km in size which corresponds to a localized Bouguer gravity anomaly in excess of –95 mG [*Finn et al.*, 1991]. We informally designate this as the Muckleshoot basin (Figures 6a–6d), after the Muckleshoot Native American Reservation which is located near the center of the basin. The Washington State borehole penetrates nearly 4 km of Eocene and younger sedimentary and volcaniclastic rocks in the southern end of the Muckleshoot basin (Figure 1) [*Johnson et al.*, 1994; *Brocher and Ruebel*, 1998]. Although ray path constraint is poor in the top few kilometers, and resolution in the vicinity of the basin is reduced, particularly at the 10 km cell spacing (Figure 3b), the independent observations of gravity and borehole data are consistent with the shape and depth of this low velocity feature from our tomography.

[36] Above 4 km depth, velocities in the Muckleshoot basin are higher than rocks at similar depths in the adjacent Seattle and Tacoma basins. However, at 7 km depth the Muckleshoot basin velocity is lower than that of the Tacoma basin. The eastern boundary trends N–S beneath the foothills of the Cascades where higher velocity rocks (5–6 km/s), most likely representing the Cascade basement, are encountered. From model PS3DA, the basin reaches a maximum depth of approximately 7–9 km (Figure 4a), approximately 80% of the depth of the Seattle basin.

4.1.4. Seattle Fault Zone (SFZ)

[37] The northern boundary of the SVH is marked by steep velocity and gravity gradients corresponding to the SFZ. Seismic reflection profiles in Puget Sound reveal a 5-km-wide deformation zone within the upper few kilometers of the SFZ, interpreted by *Johnson et al.* [1994, 1999] and by *Pratt et al.* [1997] as a multisegmented, southward-dipping thrust fault. Our tomography results suggest that the main SFZ strikes WNW (Figures 6b and 6c) and is subparallel to the Tacoma fault. In cross-section, velocity contours are nearly vertical in places where structural relief is the greatest (Figure 5b, 70 N). Although resolution from tomography is not sufficient to determine fault dip, our results are consistent with a high-angle boundary, and possibly a thrust fault with southward dip. The steepest lateral velocity gradient is visible in N–S cross-section beneath Puget Sound from Bremerton to West Seattle

Figure 7. (opposite) Interpretive horizontal section showing the velocity model at 2.5 km depth. Thick dashed red lines show our interpretation of fault locations from the tomography; thin dashed red lines show locations or limits of faults inferred from *Johnson et al.* [1994, 1996, 1999] and *Gower et al.* [1985]. The Toe Jam Hill fault scarp is labeled and shown as a solid red line. Blue triangles pointing up (Δ) are locations of uplift and blue triangles pointing down (∇) are locations of subsidence dated approximately 1100 years ago [*Bucknam et al.*, 1992]. All relocated earthquakes are shown as open circles with magnitude scale in the lower left corner. Abbreviations: BH—Blue Hills; CVH—Carnation velocity high; DB—Dabob Bay; DDMF—Darrington-Devils Mountain fault zone; OF—Olympia fault; PB—Possession basin; PLVH—Port Ludlow Velocity High; PTB—Port Townsend basin; RP—Restoration Point; SqB—Sequim basin; SqF—Sequim fault; SVH—Seattle velocity high; SWIF—Southern Whidbey Island fault zone.

(62–75 E) and persists to a depth of approximately 10 km. Velocity gradients across the fault west of 62 E are more gradual except directly north of the Blue Hills (45 E) where contours are nearly vertical for 2–3 km. We are unable to identify vertical displacement on the SFZ any further west than Hood Canal near coordinates (40, 80). At this location, a strong lateral velocity gradient forms the abrupt western boundary of the Seattle basin which we interpret to be the western end of the SFZ. Velocity contours east of Lake Washington reveal limited vertical relief across the fault (Figure 5c) and there is little evidence for structural relief east of 100 E, which we interpret to be the eastern extent of the tomographically resolved SFZ.

4.1.5. Seattle Basin

[38] The Seattle basin contains Eocene–Oligocene and younger sedimentary rocks, and has a negative Bouguer gravity anomaly exceeding -120 mG [Danes *et al.*, 1965; Finn *et al.*, 1991]. Based on high-resolution seismic reflection profiling from the SHIPS experiment plus gravity modeling, *ten Brink et al.* [2002] detailed the evolution of the Seattle basin and fault, with deformation beginning in Middle Miocene. In the upper 2 to 3 km of model PS3DA, the dimensions of the Seattle basin are approximately 70 km E–W and 25 km N–S, extending from Hood Canal to nearly the Cascade foothills (Figures 6a and 6b). The deepest part of the Seattle basin, as defined by the 5.5 km/s P wave iso-velocity surface, occurs beneath Seattle at 9–10 km depth (Figure 6e, coordinates (80, 70)). Deeper than 7 km, the basin has a NE trending arcuate structure, which may reflect the extension of the basin around the east end of the Kingston arch (Figures 6d and 6e). Previous estimates of the basin-depth have been 7.5 km [Pratt *et al.*, 1997] and 9–10 km [Danes *et al.*, 1965; Johnson *et al.*, 1994; Brocher *et al.*, 2001]. The northern boundary of the Seattle basin in our model is formed by the Port Ludlow velocity high and the Kingston arch [Pratt *et al.*, 1997; Brocher *et al.*, 2001]. The western edge of the basin appears to be sharply truncated beneath Dabob Bay, coincident with a sharp NNW trending velocity gradient (Figures 6a–6c) which we interpret to be a fault.

4.1.6. Port Ludlow Velocity High (PLVH), Kingston Arch, and Possession Basin

[39] The PLVH is centered at coordinates (50, 115) in the northwestern portion of model PS3DA (Figures 6a–6c), and corresponds to a roughly rectangular, and slightly positive, Bouguer gravity anomaly [Finn *et al.*, 1991]. Velocities within the PLVH are as high as 6.0 km/s at 4 km depth which we interpret as Crescent basement at shallow depth. This feature was termed the “Port Ludlow uplift” by Brocher *et al.* [2001], but, like the SVH, we prefer the descriptive name PLVH. The northern boundary of the PLVH corresponds to the Sequim fault, an E–W trending structure described in part by Johnson *et al.* [1996] and named by Brocher *et al.* [2001]. Using the 4.5 km/s velocity contour as an approximate guide to the location of the Sequim fault, we trace it to the west from the PLVH as an arcuate feature lying along a sharp velocity gradient with relative north side down displacement. The fault appears to bound the south end of the Port Townsend basin and can be traced no further west than 20 E. This location for the fault is consistent with outcrops of basalt to the south near Discovery Bay [Tabor and Cady, 1978a].

[40] The eastern boundary of the PLVH is a steep velocity gradient which trends NNW and was interpreted as a possible fault by Brocher *et al.* [2001]. The steepness of this gradient most likely represents a fault (Figures 4c and 7) that does not appear to extend further south than the PLVH or further north than the Sequim fault. Crescent basalts are exposed at the surface in a quarry in the southeast corner of the PLVH. Basalts were also encountered at 1 km depth in the Pope-Talbot #18-1 well, and only a few kilometers to the southeast on the Kingston arch at the Mobil-Kingston #1 well, the basalts are more than 2 km deep (Figure 1) [Brocher and Ruebel, 1998]. These observations provide an independent constraint for the varying depth and composition of this basement structure. Due to a lack of ray path constraint north of Dabob Bay, the boundary between the Crescent basalts exposed at the surface on the Olympic Peninsula and the western portion of the PLVH (Figures 4c, 6b, and 6c) cannot be resolved in the upper 2–3 km. However, below 2 km depth velocities north of Dabob Bay are slightly less than adjacent velocities in the PLVH to the west. At 4 km depth and below, rocks in the PLVH are continuous with Crescent rocks northwest of Dabob Bay.

[41] The southern boundary of the PLVH was interpreted to be a fault by Brocher *et al.* [2001] (the Lofall fault). The velocity gradients observed at this location are less than those areas in our model where faults are more likely to exist. As a result, we cannot distinguish from the model alone whether this feature is a fault or a fold. The southeast corner of the PLVH merges with the Kingston arch, an E–W trending shallow high velocity anomaly which bounds the northern Seattle basin and is interpreted as an anticlinal fold [Johnson *et al.*, 1994, 1996; Pratt *et al.*, 1997]. We have imaged the Kingston arch as a WNW trending feature approximately 10 by 25 km in dimension (Figures 6a–6c and 7), which appears to plunge eastward, consistent with the interpretation of Gower *et al.* [1985], and appears to be the eastward extension of the PLVH. Constant velocity surfaces dip gently southward (10° – 20°) on the south side of the arch, and higher velocity Crescent rocks are at 2.1 km depth at the crest as identified in the Mobil-Kingston #1 borehole (Figure 1). The eastward-dipping structure of the arch is distinct from the basin velocities to approximately 80 E at 6 km depth (Figure 6c).

[42] There are several similarities between the PLVH and the SVH to the south. Both structures are roughly rectangular and have similarly high velocities representing relatively shallow Crescent basement with sedimentary basins bounding three sides. Both features appear to be connected westward to the uplifted Crescent formation on the Olympic Peninsula.

[43] The northern slope of the Kingston arch forms the southern boundary of a small unnamed basin composed of Eocene–Oligocene to Quaternary sedimentary rocks [Johnson *et al.*, 1996; Pratt *et al.*, 1997] which we informally designate as the Possession basin (coordinate (70, 110)). This basin is slightly elongated E–W and is approximately 25 by 15 km (Figures 4c, 5b, 6a–6c, and 7). The western boundary of the basin is defined by distinct gravity and velocity gradients where the basin is structurally juxtaposed to the PLVH. The northern boundary of the basin is not well imaged in the upper 1–2 km of our model, but seismic

reflection data suggests that the N and NE boundaries of the basin are formed by the southern Whidbey Island fault [Johnson *et al.*, 1996]. The basin does not appear to extend much further east than Puget Sound (Figure 6), but ray path coverage is poor in this part of the model. We estimate the maximum basin depth to be approximately 5–6 km at coordinates (70, 112) (Figure 5b).

4.1.7. Southern Whidbey Island and Coast Range Boundary Faults

[44] The southern Whidbey Island fault zone (SWIF), proposed by Johnson *et al.* [1996] from seismic reflection and gravity data and correlation of boreholes (Figure 1), is interpreted to represent the crustal boundary between the pre-Tertiary Cascade basement on the northeast and the Coast Range basement on the southwest. The Cascade basement was penetrated northeast of the SWIF in the Silvana Community #12-1 borehole (Figure 1) at 2.2 km depth and the measured P wave velocity was 5.5 km/s on average [Brocher and Ruebel, 1998]. Unfortunately, the similar velocities of Crescent and Cascade basement rocks does not provide enough velocity contrast to clearly distinguish between these two provinces using tomography. The location of the SWIF, described by Johnson *et al.* [1996], appears in our model to form the northeastern boundary of the Port Townsend basin (Figures 6a–6c, 7) where it trends NW toward Victoria (Figure 1) [Brocher *et al.*, 2001]. In cross-section, however, this boundary appears to be gradual (Figure 5a). Tracing the inferred location of the fault to the southwest in model PS3DA, no obvious vertical structure on the fault is apparent.

[45] The existence and general location of the Coast Range boundary fault (CRBF) has been inferred by Johnson [1984, 1985] to lie beneath the central Puget Lowland (Figure 1) based on tectonic and sedimentologic evidence. This fault is hypothesized to represent the contact between Crescent basement to the west and pre-Tertiary Cascade basement to the east. Velocity contrasts across the contact may be minimal because of similar basement velocities and comparable velocities in the shallow structure, particularly if the fault has been inactive since the Eocene [Johnson *et al.*, 1996]. Our model, PS3DA, shows no basement velocity contrast at the location of the hypothesized CRBF.

4.1.8. Crescent Basement

[46] Velocities in the shallowest regions of the model west of Hood Canal and in the Blue Hills range from 5.0 to 6.0 km/s where the Crescent formation is exposed at the surface (Figure 1), consistent with our interpretation of Crescent basalt velocities in the upper 5 km of the model. At 4 km depth (Figure 6c) we interpret velocities in excess of 5.0 km/s in the western half of the model to be Crescent basement, which are most prominent west of Hood Canal, and in the SVH and PLVH. In E–W cross-section (Figure 4b), the Crescent basement forms a concave-upward structure which can be traced to outcropping basement in the eastern Olympics.

[47] The Crescent basement appears to extend to the maximum depth resolved in our model, giving it a thickness of 20 km or more over much of our model area (Figures 4 and 5). Below 7 km depth, the model is dominated by velocities in excess of 5.5 km/s, with localized anomalies having velocities as high as 7.0–7.5 km/s (Figures 6d–6h).

Velocity magnitudes may be overestimated by a few percent but velocities of 7 km/s and above are too high to represent basalt. It is also unlikely that we have imaged the base of the continental crust at these depths, which is more than 40 km deep on the west flank of the Cascades where upper mantle velocities are 7.6–7.8 km/s or higher [Schultz and Crosson, 1996; Miller *et al.*, 1997]. Gabbroic complexes have been observed in the Blue Hills within the SVH and within the ophiolite stratigraphy of the Metchosin igneous complex on Vancouver Island, both of which have been correlated with the Crescent formation [Massey, 1986; Haeussler and Clark, 2000]. In addition, P wave velocities of gabbro from 5 to 35 km depth range from 6.8 to 7.2 km/s [Christensen and Mooney, 1995], consistent with observed high velocities in model PS3DA. We therefore interpret velocities in excess of 7 km/s in our model as higher velocity gabbro emplaced within the Crescent formation, an interpretation also made by Parsons *et al.* [1999].

4.1.9. Additional Structures

[48] The existence and inferred location of the Hood Canal fault is based on gravity and topographic features along Hood Canal (Figure 1) [Gower *et al.*, 1985]. This fault presumably separates the Crescent formation exposed at the surface west of Hood Canal from Quaternary sedimentary rocks to the east. E–W cross-sections through the model reveal the Crescent basement dipping uniformly eastward from surface exposures west of Hood Canal (Figure 4b, 30 E) with no apparent vertical offset, raising questions about the existence of the Hood Canal fault. Although strike-slip or small vertical offsets at this location cannot be ruled out by our tomography model, the inferred east-side-down structure along the full length of Hood Canal [Brocher *et al.*, 2001] is not supported by our model. However, along a 10–15 km length stretch on the west side of Dabob Bay (coordinates (40, 95)) a steep velocity gradient is consistent with faulting in which the east side is displaced downward with respect to near surface Crescent formation on the west side (Figures 6a and 6b). This fault segment may be the west margin of the Seattle basin and it may be effectively a short continuation of the Seattle fault northwestward from its western end. North of Dabob Bay, it is unclear from the tomographic model whether this structure continues northward into the inferred location of the Hood Canal–Discovery Bay fault zone [Johnson *et al.*, 1996], but our model does not suggest a significant lateral velocity gradient in this region.

[49] Northwest of the PLVH and west of the Sequim fault is a small, low velocity structure which we informally designate as the Sequim basin (Figures 6a and 6b, coordinates (13, 35)). This basin was also imaged by Ramachandran [2001] in a study utilizing SHIPS data. The basin is elongated WNW and corresponds to a similarly shaped Bouguer gravity anomaly [Finn *et al.*, 1991]. We are unable to estimate the lateral dimensions of the basin due to insufficient ray path coverage on the south, but the gravity observations suggest that this feature may extend westward beyond the edge of our model. The northern boundary of the basin is a fairly sharp velocity and gravity gradient which may be an E–W trending fault, with south-side-down. Near-surface velocities on the north side of this gradient are in excess of 4.5 km/s, and we interpret them to be Crescent basement, consistent with the nearby Dung-

ness Spit borehole (Figure 1) where basalt was encountered at 1.5 km depth. We estimate the basin to have a maximum depth of 3 to 4 km (Figure 6).

[50] Lack of ray coverage in the upper 5–6 km of the northeastern region of our model prevented us from imaging much of the Everett basin. The shallowest structure of the basin is visible in Figure 6a where it appears as a NW trending elliptical feature, northeast of the SWIF (Figure 7). The limited tomography picture is consistent with Bouguer gravity observations [Finn *et al.*, 1991].

[51] Approximately 20 km east of the Seattle basin at the foothills of the Cascades, near coordinates (120, 90), is a subcircular high velocity anomaly approximately 10 km in diameter. We will refer to this anomaly as the Carnation velocity high (CVH, Figures 4b, 6a, 6b, and 7). Although it corresponds well with the general increase in velocity in this part of the model, the CVH includes an apparently isolated core, extending 5 to 7 km in-depth, with velocities as high as 7.0 km/s. Our resolution tests suggest good resolution in this region at the 15 km grid spacing (Figure 3a) with somewhat reduced resolution at 10 km grid spacing. Further investigation of the data constraints on this anomaly have failed to reveal any potentially corrupted data that might explain the existence of this feature. Hence, we tentatively accept this anomaly as real. The CVH does not correspond to any known gravity or magnetic anomalies that could confirm its existence, and there are no mapped mafic exposures in its immediate vicinity. However, small outcrops of metagabbro are mapped approximately 20 km to the east and southeast of this feature [Tabor *et al.*, 1993] and such rocks could produce these high velocities if they were more extensive in the subsurface.

4.2. Relocated Earthquakes and Focal Mechanisms

4.2.1. Earthquake Locations

[52] A total of 912 earthquakes were relocated in the joint tomographic inversion. Comparison of the 3-D locations with the starting 1-D locations reveals a mean absolute epicentral change of 970 m and a deepening of hypocentral depths of 235 m on average. Since the average distribution of hypocenters did not change significantly from 1-D to 3-D models, the 1-D model appears to be a good regional average of the 3-D model. Our earthquake data set contains only well located, typically larger and tectonically significant events selected from the complete catalog of PNSN earthquakes. Comparison of our resulting location distribution with the complete catalog distribution containing smaller and less well located earthquakes indicates that the events in our data set are representative of the overall pattern of seismicity for the model region.

[53] Since our model region is smaller than the PNSN regional network in western Washington, some network stations normally used for 1-D model locations were excluded from the inversion. As a result, the distance to the nearest station and the azimuthal gap for some earthquakes was degraded. We recalculated the azimuthal gaps for the 3-D hypocenters and determined that 179 events (approximately 20%) had gaps larger than 160°. Our confidence in the locations of these events is somewhat reduced and they are distinguished on Figure 2 from events with gaps less than 160°, which we classify as well located. Nearly all of these lower confidence events are near the

borders of the model on the north and east, mostly located within the Cascade terrane.

4.2.2. Focal Mechanism Determination

[54] A subset of relocated earthquakes were selected for focal mechanism analysis which were either: (1) included within the Seattle, Tacoma, or southern Whidbey Island fault zones with magnitudes greater than 2.2, or (2) had magnitudes greater than 3.0, regardless of location. The three fault zone regions are illustrated by dashed rectangles on Figure 8 and the earthquakes greater than magnitude 3 are listed in Table 3. Focal mechanisms for these events were determined by P wave raytracing using one of two 1-D velocity models, chosen to be representative of the 3-D velocity structure depending on the location of the event. The model used for events in the Seattle and Tacoma fault zones was derived by fitting linear velocity model trends through vertical samples taken from six central locations in the 3-D model (Figure 8; “Seattle Model” in Table 4). Mechanisms for events outside the Seattle and Tacoma fault zones were determined using samples taken from four outlying and two central locations in the model (“North/East Model” in Table 4).

4.2.3. Regional Seismicity and Focal Mechanism Characteristics

[55] Earthquake locations are shown with magnitude coding on Figures 6–7 and Figure 9. The most concentrated seismicity occurs between 15 and 25 km depth within what we interpret to be the Crescent basement in the central part of the model (Figure 9b). Earthquakes are generally sparse in the upper 10 km of the crust, but in the central part of the model, corresponding to the SVH where Crescent basement approaches the surface, hypocenters occur at shallower depths. In the central and western parts of the model, at depths less than 10 km earthquakes are nearly absent north of the SFZ, and virtually no seismicity is observed south of the Tacoma basin (Figures 9a and 9b). In the westernmost region (Figure 9a), the base of crustal seismicity decreases in-depth northward to approximately 130 N. In the central part of the model, shown in Figure 9b, there is a distinct concave upward pattern in the deepest crustal seismicity south of the SWIF, with the largest concentration of events beneath the Seattle basin. Pratt *et al.* [1997] proposed a midcrustal decollement as a fundamental component of their thrust sheet hypothesis for the origin of the Puget Lowland faults and basins. The seismicity pattern and velocity structure shows no direct evidence for this midcrustal feature, so if decoupling occurs on a subhorizontal decollement, it has no apparent effect on the contemporary earthquake activity and is without clear structural manifestation.

[56] East of Lake Washington (Figure 9c), the zone of concentrated seismicity observed in the Crescent basement is absent and earthquakes are more uniformly distributed from near the surface to more than 25 km depth. We interpret this change to reflect the eastward transition into the Cascade basement, which is compositionally distinct from the Coast Range basement and in most places lacks a thick sedimentary cover. A similar change in seismicity is observed north of the SWIF where the number of earthquakes decreases and the events are more uniformly distributed in depth (Figures 9a and 9b). We believe these changes may also be a seismic signature of the northward transition to the Cascade province. Shallow earthquakes

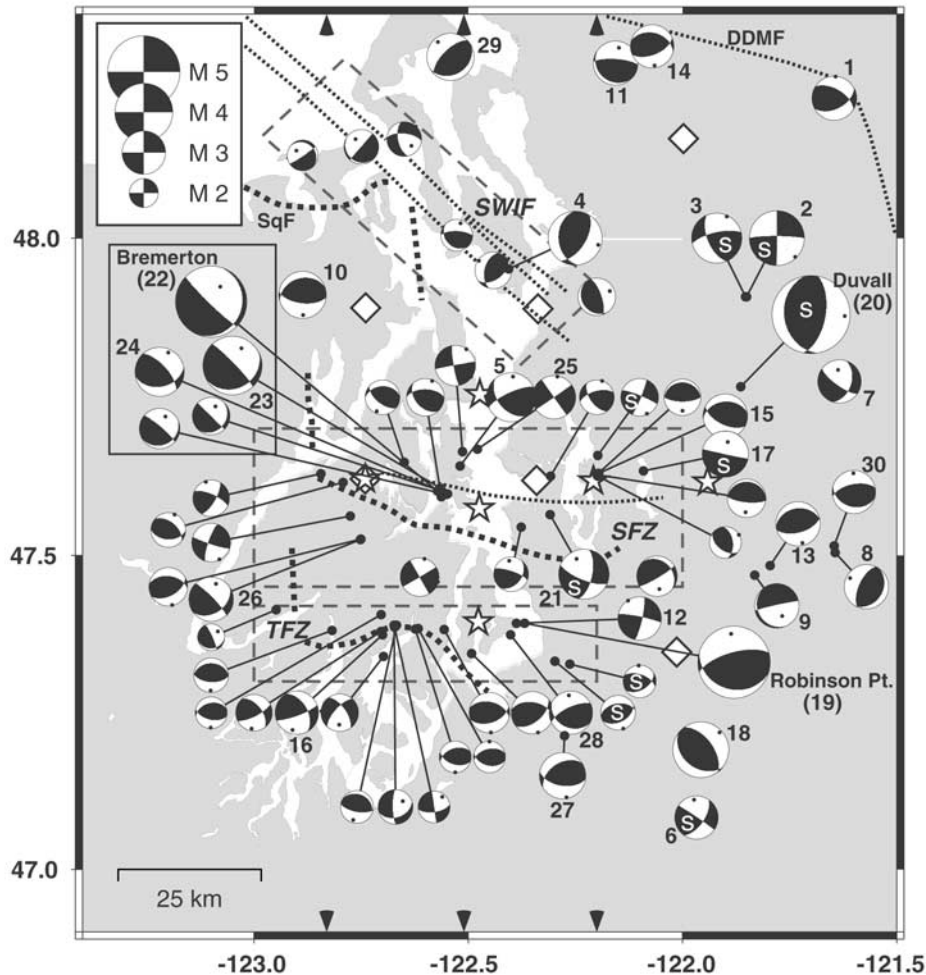


Figure 8. Map of selected earthquakes with well constrained focal mechanisms plotted using equal-area, lower-hemisphere projections. Numbered mechanisms are events greater than magnitude 3 corresponding to events listed in Table 3. Black dots in dilatational quadrants are projected P-axes for each event and mechanisms labeled with an “s” are shallow events less than 10 km deep. Thick dashed lines show fault locations inferred from the tomography; thin dashed lines show locations or limits of faults inferred from Johnson *et al.* [1994, 1996, 1999]. Grey dashed boxes show areas used to select events for focal mechanism analysis. Abbreviations: DDMF—Darrington-Deviils Mountain fault; SFZ—Seattle fault zone; SWIF—Southern Whidbey Island fault zone; TFZ—Tacoma fault zone. Stars show sampling locations from the 3-D model for construction of the Seattle 1-D velocity model; diamonds show sampling locations for construction of the North/East 1-D model (see text and Table 4). Pointers on axes show locations of cross-sections shown in Figure 9.

appear within the eastern portion of the Seattle basin, unlike the central and western portions, reflecting possible structural and tectonic changes within the basin.

[57] The majority of focal mechanisms were determined from earthquakes occurring in the Crescent basement. Virtually no earthquakes occur in regions which we interpret to be within the OSC, and relatively few earthquakes occur within the shallow sedimentary basins. Overall, focal mechanism solutions reveal primarily strike-slip and thrust mechanisms with P-axes trending N–S with an overall average plunge of less than 20° (Figure 10), suggesting that regional maximum compressive stress is aligned N–S and is nearly horizontal. These results are consistent with the results of Ma *et al.* [1996].

[58] Focal mechanisms for 12 earthquakes with magnitudes greater than 3.0 located outside the Tacoma, Seattle, and southern Whidbey Island fault zones were determined (Figures 8 and 9), and all but one of these events appear to be located within the Cascade province. Mechanisms of these events are mainly oblique thrust and strike-slip with P-axes plunging shallowly and trending N–S.

[59] Two clusters of earthquakes in the northeastern part of the model are located in the vicinity of the eastern extent of the Darrington-Deviils Mountain fault (DDMF)—a region of very sparse seismicity. Three focal mechanisms were determined for the largest of these earthquakes (Figure 8; Events 1, 11, and 14 of Table 3) which have depths between 10 and 16 km. All three mechanisms are consistent with N–S

Table 3. Relocated Hypocenters and Focal Solutions for Earthquakes Greater Than Magnitude 3.0

No. ^a	Date, UT	Latitude, °N	Longitude, °W	Depth, km	Magnitude	P-Axis ^b		T-Axis ^b		Plane A ^c		
						Az	Pl	Az	Pl	Sk	Dp	Rk
1	22 August 1980	48.219	121.645	11.25	3.1	3	4	266	56	-59	57	131
2	19 September 1980	47.908	121.851	5.22	3.8	135	4	225	5	0	89	6
3	21 September 1980	47.908	121.853	5.16	3.5	25	7	119	35	-103	71	31
4	12 November 1981	47.952	122.405	26.73	3.7	107	11	345	69	32	58	111
5	12 April 1982	47.641	122.519	27.70	3.4	6	18	114	43	-115	75	47
6	24 January 1983	47.083	121.967	4.02	3.0	353	18	255	21	-56	88	152
7	25 May 1983	47.775	121.634	11.97	3.0	354	45	245	18	125	74	-131
8	12 August 1983	47.504	121.644	15.16	3.1	297	17	107	73	-155	62	87
9	5 October 1983	47.469	121.832	24.13	3.1	153	47	0	40	-103	86	-104
10	11 January 1985	47.911	122.887	21.31	3.3	178	15	36	72	97	61	102
11	5 March 1985	48.274	122.156	15.44	3.1	12	29	170	60	-86	75	80
	16 June 1985	47.439	121.840	17.83	3.1							
	6 July 1985	47.732	122.221	19.25	3.1							
12	14 September 1985	47.393	122.387	18.68	3.0	327	2	236	12	-79	83	170
13	30 December 1990	47.484	121.795	18.99	3.1	167	13	333	77	74	58	86
	18 January 1992	47.405	122.710	13.18	3.1							
14	20 January 1992	48.300	122.071	13.10	3.0	173	11	293	69	68	58	69
15	29 March 1992	47.630	122.196	27.83	3.1	193	12	67	70	116	59	108
16	26 January 1993	47.374	122.700	26.07	3.0	194	19	299	36	70	79	41
17	22 July 1994	47.634	122.091	8.83	3.2	12	46	192	44	102	89	-90
18	10 September 1994 Robinson Point	47.191	121.957	18.32	3.9	47	10	263	77	-36	55	99
19	29 January 1995	47.393	122.368	16.38	5.0	355	21	140	65	-106	67	76
	30 March 1996 Duvall ^d	47.322	122.433	14.77	3.0							
20	3 May 1996	47.767	121.864	9.06	5.4	93	14	305	73	10	60	100
	3 May 1996	47.776	121.878	9.17	3.0							
21	10 February 1997 Bremerton	47.565	122.309	5.15	3.5	334	33	241	6	112	72	-151
22	23 June 1997	47.602	122.572	11.45	4.9	31	49	235	38	134	85	-102
23	27 June 1997	47.606	122.565	10.74	4.1	27	35	249	47	-44	84	112
24	11 July 1997	47.597	122.548	10.08	3.4	24	16	268	55	-43	67	123
25	12 February 1998	47.668	122.478	24.34	3.0	190	1	279	2	55	89	0
26	3 November 1998	47.525	122.751	22.77	3.1	17	27	260	41	-44	82	127
27	4 January 1999	47.214	122.275	25.97	3.2	170	5	69	67	100	54	118
28	2 July 1999	47.374	122.401	21.47	3.0	353	20	120	59	-115	69	65
29	1 November 2000	48.283	122.541	22.18	3.3	320	19	123	70	-135	64	84
30	31 December 2000	47.515	121.646	14.98	3.0	359	14	138	70	-102	60	75

^aLabel number refers to numbered focal mechanisms shown in Figures 8 and 9.

^bAxes orientation given as azimuth (Az) in degrees clockwise from the north and degrees plunge (Pl) from horizontal.

^cOrientation of nodal plane A from double-couple solution in degrees strike (Sk), dip (Dp), and rake (Rk) (plane A is not necessarily the preferred fault plane). Strike angles less than zero are measured counterclockwise from the north.

^dDuvall focal mechanism taken from PNSN catalog solution.

compression. The occurrence of these earthquakes suggests possible activity associated with the DDMF, which has recently been postulated to be an active fault by *Johnson et al.* [2001] on the basis of geologic and seismic reflection data. However, the mechanisms of these deeper earthquakes are not consistent with the left-lateral component of motion postulated by *Johnson et al.* [2001] for the DDMF. Unfortunately, our velocity model is poorly constrained in this region due to proximity to the model boundary, preventing possible delineation of the fault from velocity variation.

4.2.4. Tacoma Fault Zone (TFZ)

[60] On the western side of our model at depths less than 10 km (Figure 9a) a cluster of earthquakes appearing as a subvertical lineation may be associated with the TFZ (coordinate 60 N). If these events indeed reflect displacement on the TFZ, they are consistent with a high angle, possibly north-dipping, fault zone extending to at least 10 km depth and possibly deeper. We suggest caution however, in interpreting such shallow nearly vertical distributions of hypocenters since depth constraint is often poor in the upper 10 km of the crust, and such vertical patterns may be, at least

Table 4. 1-D Velocity Models Used to Compute Focal Mechanisms

Depth Range, km	Seattle Model P-Velocity, km/s	North/East Model P-Velocity, km/s
0.0–0.5	3.20	3.62
0.5–1.5	3.49	3.88
1.5–2.5	3.78	4.13
2.5–3.5	4.08	4.39
3.5–4.5	4.37	4.64
4.5–5.5	4.66	4.90
5.5–6.5	4.96	5.16
6.5–7.5	5.25	5.41
7.5–8.5	5.54	5.67
8.5–9.5	5.84	5.92
9.5–10.5	6.13	6.18
10.5–11.5	6.42	6.44
11.5–14.5	6.46	6.48
14.5–17.5	6.49	6.53
17.5–20.5	6.51	6.57
20.5–23.5	6.54	6.62
23.5–26.5	6.57	6.66
26.5–29.5	6.59	6.71
29.5–32.5	6.62	6.76
32.5–35.5	6.65	6.80
35.5–40.0	6.67	6.85

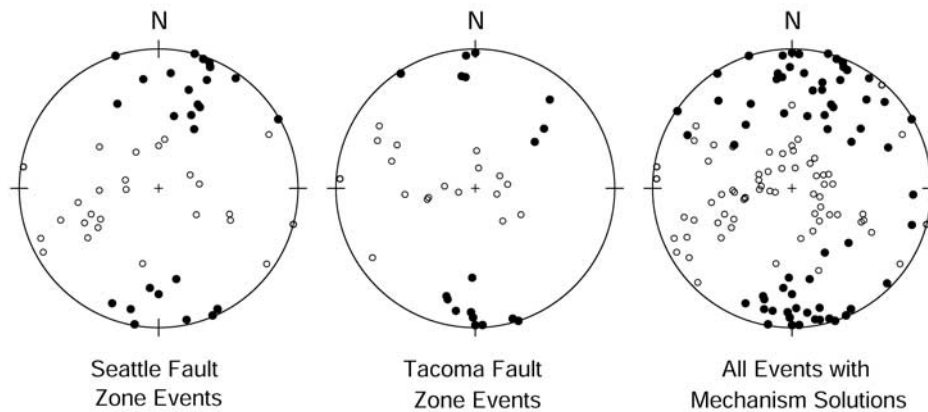


Figure 10. Equal-area, lower-hemisphere projections of P-axes (●) and T-axes (○) in the Seattle and Tacoma fault zone regions and all mechanisms done in this study. The Seattle and Tacoma fault zone regions are delineated by the appropriate dashed rectangles of Figure 8.

solution reported by *Dewberry and Crosson* [1996] (Event 19, Figures 8 and 9b and Table 3).

4.2.5. Seattle Fault Zone (SFZ)

[62] There is a greater frequency of shallow (<10 km depth) seismic activity associated with the SFZ than with the TFZ. Seismicity is distributed over a broad zone and is not localized to one or more narrow faults, suggesting that the SFZ is a complex structure. The western and eastern ends of the fault (Figures 9a and 9c) show increased activity in the upper 10 km of the crust relative to the central portion of the fault (Figure 9b). Seismicity in the SFZ does not show evidence of alignment along the proposed south-dipping thrust model of *Johnson et al.* [1994, 1999] and *Pratt et al.* [1997].

[63] A total of 26 focal mechanisms were determined for earthquakes near the SFZ; these are predominantly oblique thrust or strike-slip mechanisms (Figure 8). Nodal planes for thrust mechanisms strike generally E–W with most solutions slightly rotated NW–SE. P-axes for the SFZ events are generally oriented NNE or S and plunge shallowly at 18° on average; T-axes have a broader plunge distribution averaging 42° and trending mostly west to vertical (Figure 10).

[64] The magnitude 4.9 Bremerton earthquake was relocated in the joint inversion to a depth of 11.5 km. Our computed focal mechanism for this event has one nearly vertical nodal plane striking NW with oblique normal offset and one shallowly dipping nodal plane striking NNE with oblique strike-slip offset (Event 22, Figures 8 and 9b and Table 3). Focal mechanisms for four aftershocks from the Bremerton event reveal similarly oriented nodal planes as the main shock but with slightly larger strike-slip or thrust components (Figure 8). The location of the Bremerton earthquake relative to its aftershocks reveals a vertical distribution of nearly 8 km with a lateral E–W scatter of 3 km and virtually no lateral N–S variation. Lack of strong depth constraint for this sequence because of suboptimal station distribution may contribute in part to the vertical spread of hypocenters. Nevertheless, the aftershock pattern is most consistent with the nearly vertical nodal plane as the true fault. If the vertical plane ruptured, then the overall motion is north-side-up and eastward with respect to the south side of the fault.

[65] Only three focal mechanisms within the SFZ are from earthquakes shallower than 10 km (Figure 8). Two of these shallow events have mechanisms similar to the Bremerton earthquake—Event 21 is directly beneath the city of Seattle (Figures 8 and 9c and Table 3) and Event 17 is slightly north of the deformation front defined by *Blakely et al.* [2002] with vertical and horizontal nodal planes with either north-side-up or thrust offset. The remaining shallow event, at a depth of 5 km, is located beneath the east side of Lake Washington and is almost purely strike-slip with nodal planes oriented NNE and WNW (Figure 8).

[66] The most significant shallow earthquakes within the general region of the SFZ have occurred within or below the Seattle basin and are consistent with evidence of north-side-up displacement. The E–W trending Toe Jam Hill fault scarp on southern Bainbridge Island [*Blakely et al.* 2002] is a north-dipping, north-side-up structure directly above the Bremerton earthquake sequence. *Blakely et al.* [2002] propose that the fault scarp is either the result of a roof-thrust within the SFZ or is the result of movement on a nearly vertical fault deep within the Seattle basin. We believe that the latter interpretation is most consistent with the observed seismicity and focal mechanism evidence. Both gravity evidence and corroborating seismic velocity evidence demonstrates that the Seattle basin is a large local mass deficiency, which is at least locally, and probably regionally, isostatically uncompensated. We suggest that isostatic body force (buoyancy) may presently be elevating the basin producing displacement in or near the SFZ where the basin is both deepest and fault bounded to a depth of at least 10 km. This scenario is consistent with the locations and focal mechanisms of shallow events within the SFZ. Isostatic forces tending to elevate the Seattle basin must coexist with arc-parallel tectonic compressive stress resulting from oblique subduction as proposed by *Wang et al.* [1997]. The relative roles of these two tectonic mechanisms are unknown, but are clearly important in understanding the nature of the SFZ and the earthquake hazard that it presents.

4.2.6. Southern Whidbey Island Fault Zone (SWIF)

[67] Only one earthquake of magnitude greater than 3.0 has occurred in the general vicinity of the SWIF since

1980 (Event 4, Table 3). We determined seven well constrained mechanisms from a larger region containing the SWIF (Figure 8). Hypocentral depths of these events are greater than 14 km and their focal mechanisms are mainly thrust with a variety of nodal plane orientations. Although they may be related to the SWIF, we find no evidence in the location or orientations of these earthquakes to directly correlate them to the fault, particularly because they occur significantly deeper than the region of the fault zone imaged by seismic reflection profiles [Johnson *et al.*, 1996].

5. Summary and Conclusions

[68] High-resolution 3-D seismic tomography using both explosion and earthquake data provides a detailed P wave velocity image of the Puget Lowland to a depth of 30 km. The Lowland is characterized by six distinct basins varying in depth from 3 to 10 km (Figure 7). The basins are separated by high velocity regions where Crescent formation rocks are typically within one or two kilometers of the surface. In addition to the Seattle, Tacoma, Port Townsend, and Possession basins which have been previously described, we have described the Muckleshoot and Sequim basins which have not formerly been delineated as distinct basins.

[69] The Seattle fault zone is a WNW trending zone of rapid lateral velocity transition from the low velocity sedimentary rocks of the Seattle basin to the high velocity region separating the Seattle and Tacoma basins. The combination of tomography, seismicity, and focal mechanisms suggest that the SFZ is a complex zone of deformation, rather than a single narrow fault, with north-side-up displacement perhaps driven by isostatic readjustment of the low density basin. The SFZ is truncated on the west beneath Hood Canal and seismography provides no supporting evidence for extension of the fault eastward of Lake Sammamish.

[70] The Seattle and Port Ludlow velocity highs are strikingly analogous, suggesting similar processes of formation. The Kingston arch appears to be an anticlinal fold which at depth is the southeastward extension of the Port Ludlow velocity high. Whether these velocity highs represent basement that has been structurally elevated, or basement that has remained at relatively constant postemplacement depth while the adjacent basins subsided cannot be directly ascertained by tomography but is a question remaining for further tectonic investigation.

[71] Additional shallow faults inferred from our model include: the arcuate and apparently steeply dipping Tacoma fault zone; N–S trending faults beneath Dabob Bay and to the east of the Port Ludlow velocity high; the arcuate Sequim fault south of the Port Townsend basin; and a possible E–W trending fault north of the Sequim basin.

[72] Earthquakes jointly relocated during our inversion are not significantly different on average from the 1-D model locations. These earthquakes reveal a midcrustal zone of concentrated seismicity between 15 and 25 km depth occurring mainly within the Crescent basement which arches beneath the Lowland from its surface exposure on the Olympic Peninsula. Shallower hypocenters are found near the Seattle and Tacoma fault zones. Although these

earthquakes do not clearly delineate individual fault surfaces, this localization of seismicity indicates a tectonically active region of the Lowland which reinforces the potential seismic hazards associated with the Seattle and Tacoma fault zones.

[73] Our investigation provides a reference 3-D P wave velocity model (PS3DA) for future earthquake location studies, structure studies, and tectonic interpretation. Velocity variations within the Puget Lowland reveal a complex three-dimensional structural pattern that is not easily explained by simple tectonic models. Computed earthquake focal mechanisms indicate that N–S regional tectonic compression is important and is active in both thrusting and strike-slip modes of deformation. However, many features such as apparent north striking faults along the east margin of the Port Ludlow velocity high and the northern Tacoma basin, the concave-upward pattern of the basement beneath the Seattle basin, and the apparent basin-side-up focal mechanisms within the Seattle fault zone are not readily explained solely by N–S compression, requiring the consideration of additional tectonic complexity.

[74] **Acknowledgments.** Research supported by the U.S. Geological Survey (USGS), Department of the Interior, under USGS award numbers 1434-HQ-97-GR-03084, 1434-HQ-98-00017 and 99-HQ-GR-0036, and the National Science Foundation under grant EAR-0107138 to Crosson and Creager. The views and conclusions contained in this document are those of the authors and should not be interpreted as necessarily representing the official policies, either expressed or implied, of the U.S. Government. We thank the SHIPS Working Group (following individuals: M. A. Fisher, T. Parsons, R. A. Hyndman, K. C. Miller, C. N. Snelson, D. C. Mosher, T. L. Pratt, R. Ramachandran, G. D. Spence, U. S. ten Brink, A. M. Trehu, C. S. Weaver, and B. C. Zelt) for providing data, ensuring the success of the SHIPS experiments, and for advice and useful discussions. We would like to thank Harvey Greenberg for supplying digital geologic data, and Richard Stewart and Richard Blakely for helpful discussions. We are grateful to Ruth Ludwin and Brian Sherrord for early reviews of the paper, and for the comments of two anonymous reviewers who helped to significantly improve the paper.

References

- Babcock, R. S., R. R. Burmester, K. P. Clark, D. C. Engebretson, and A. Warnock, A rifted margin origin for the Crescent basalts and related rocks in the northern Coast Range volcanic province, Washington and British Columbia, *J. Geophys. Res.*, *97*, 6799–6821, 1992.
- Babcock, R. S., C. A. Suzczek, and D. C. Engebretson, The Crescent “Terrane”, Olympic peninsula and southern Vancouver Island, *Wash. Div. Geol. Earth Res. Bull.*, *80*, 141–157, (Regional Geology of Washington), 1994.
- Bakun, W. H., R. A. Haugerud, M. G. Hopper, and R. S. Ludwin, The December 1872 Washington state earthquake (abstract), *Seismol. Res. Lett.*, *72*, 269, 2001.
- Blakely, R. J., R. E. Wells, and C. S. Weaver, Puget Sound aeromagnetic maps and data, *U.S. Geol. Surv. Open File Rep.*, *99-514*, 1999.
- Blakely, R. J., R. E. Wells, C. S. Weaver, and S. Y. Johnson, Location, structure, and seismicity of the Seattle fault zone: Evidence from aeromagnetic anomalies, geologic mapping, and seismic reflection data, *Geol. Soc. Am. Bull.*, *114*, 169–177, 2002.
- Brandon, M. T., and A. R. Calderwood, High-pressure metamorphism and uplift of the Olympic subduction complex, *Geology*, *18*, 1252–1255, 1990.
- Brandon, M. T., M. K. Roden-Tice, and J. I. Garver, Late Cenozoic exhumation of the Cascadia accretionary wedge in the Olympic mountains, northwest Washington state, *Geol. Soc. Am. Bull.*, *110*, 985–1009, 1998.
- Brocher, T. M., and N. I. Christensen, Density and velocity relationships for digital sonic and density logs from coastal Washington and laboratory measurements of Olympic Peninsula mafic rocks and greywackes, *U.S. Geol. Surv. Open File Rep.*, *01-264*, 1–39, 2001.

- Brocher, T. M., and A. L. Ruebel, Compilation of 29 sonic and density logs from 23 oil test wells in western Washington state, *U.S. Geol. Surv. Open File Rep.*, 98-249, 60 pp., 1998.
- Brocher, T. M., et al., Wide-angle seismic recordings from the 1998 Seismic Hazards Investigation of Puget Sound (SHIPS), western Washington and British Columbia, *U.S. Geol. Surv. Open File Rep.*, 99-314, 110 pp., 1999.
- Brocher, T. M., et al., Report for explosion and earthquake data acquired in the 1999 Seismic Hazards Investigation of Puget Sound (SHIPS), Washington, *U.S. Geol. Surv. Open File Rep.*, 00-318, 85 pp., 2000.
- Brocher, T. M., T. Parsons, R. J. Blakely, N. I. Christensen, M. A. Fisher, and R. A. Wells, Upper crustal structure in Puget Lowland, Washington: Results from the 1998 Seismic Hazards Investigation in Puget Sound, *J. Geophys. Res.*, 106, 13,541-13,564, 2001.
- Bucknam, R. C., E. Hemphill-Haley, and E. B. Leopold, Abrupt uplift within the past 1700 years at southern Puget Sound, Washington, *Science*, 258, 1611-1614, 1992.
- Bucknam, R. C., B. L. Sherrod, and G. Elendahl, A fault scarp of probable Holocene age in the Seattle fault zone, Bainbridge Island, Washington (abstract), *Seismol. Res. Lett.*, 70, 233, 1999.
- Christensen, N. I., and W. D. Mooney, Seismic velocity structure and composition of the continental crust: A global view, *J. Geophys. Res.*, 100, 9761-9788, 1995.
- Clowes, R. M., M. T. Brandon, A. G. Green, C. J. Yorath, A. S. Brown, E. R. Kanasevich, and C. Spencer, LITHOPROBE-Southern Vancouver Island: Cenozoic subduction complex imaged by deep seismic-reflections, *Can. J. Earth Sci.*, 24, 31-51, 1987.
- Crosson, R., Crustal structure modeling of earthquake data, 2, Velocity structure of the Puget Sound region, Washington, *J. Geophys. Res.*, 81, 3047-3054, 1976.
- Danes, Z. F., M. M. Bonno, E. Brau, W. D. Gilham, T. F. Hoffman, D. Johansen, M. H. Jones, B. Malfait, J. Masten, and G. O. Teague, Geophysical investigation of the southern Puget Sound area, Washington, *J. Geophys. Res.*, 70, 5573-5580, 1965.
- Dewberry, S. R., and R. S. Crosson, The M_D 5.0 earthquake of 29 January 1995 in the Puget Lowland of western Washington: An event on the Seattle fault?, *Bull. Seismol. Soc. Am.*, 86, 1167-1172, 1996.
- Finn, C., W. M. Phillips, and D. L. Williams, Gravity anomaly and terrain maps of Washington, *U.S. Geol. Surv. Geophy. Invest. Ser. Map*, GP-988, scale 1:1,000,000 and 1:500,000, 1991.
- Fisher, M. A., et al., Results from the 1998 SHIPS Experiment, regarding urban earthquake hazards in Cascadia (abstract), *Eos Trans. AGU*, 80(46), F762, Fall Meet. Suppl., 1999.
- Gower, H. D., J. C. Yount, and R. S. Crosson, Seismotectonic map of the Puget Sound region, Washington, *U.S. Geol. Surv. Misc. Invest. Ser. Map*, I-1613, scale 1:250,000, 1985.
- Haessler, P. J., and K. P. Clark, Geologic map of the Wildcat Lake 7.5' quadrangle, Kitsap and Mason counties Washington, *U.S. Geol. Surv. Open File Rep.*, 00-356, scale 1:24,000, 1 sheet, 2000.
- Johnson, S. Y., Evidence for a margin-truncating transcurrent fault (pre-late Eocene) in western Washington, *Geology*, 12, 538-541, 1984.
- Johnson, S. Y., Eocene strike-slip faulting and nonmarine basin formation in Washington, in *Strike-Slip Deformation, Basin Formation, and Sedimentation*, no. 37, edited by K. T. Biddle and N. Christie-Blick, *Spec. Pub. Soc. Econ. Paleon. Mineral.*, pp. 283-302, 1985.
- Johnson, S. Y., C. J. Potter, and J. M. Armentrout, Origin and evolution of the Seattle Fault and Seattle Basin, Washington, *Geology*, 22, 71-74, 1994.
- Johnson, S. Y., C. J. Potter, J. M. Armentrout, J. J. Miller, C. Finn, and C. S. Weaver, The southern Whidbey Island fault: An active structure in the Puget Lowland, Washington, *Geol. Soc. Am. Bull.*, 108, 334-354, 1996.
- Johnson, S. Y., S. V. Dadisman, J. R. Childs, and W. D. Stanley, Active tectonics of the Seattle Fault and central Puget Sound, Washington—Implications for earthquake hazards, *Geol. Soc. Am. Bull.*, 111, 1042-1053, 1999.
- Johnson, S. Y., S. V. Dadisman, D. C. Mosher, R. J. Blakely, and J. R. Chiles, Active tectonics of the Devils Mountain fault and related structures, northern Puget lowland and eastern Strait of Juan de Fuca region, Pacific Northwest, *U.S. Geol. Surv. Prof. Pap.*, 1643, 45 pp., 2 sheets, 2001.
- Lees, J. M., and R. S. Crosson, Tomographic imaging of local earthquake delays times for three-dimensional velocity variation in western Washington, *J. Geophys. Res.*, 95, 4763-4776, 1990.
- Ludwin, R. S., C. S. Weaver, and R. S. Crosson, Seismicity of Washington and Oregon, in *Neotectonics of North America Decade Map*, vol. 1, edited by D. B. Slemmons, E. R. Engdahl, M. D. Zoback, and D. D. Blackwell, pp. 77-98, Geol. Soc. of Am., Boulder, Colo., 1991.
- Ma, L., R. S. Crosson, and R. S. Ludwin, Western Washington earthquake focal mechanisms and their relationship to regional tectonic stress, in *Assessing Earthquake Hazards and Reducing Risk in the Pacific Northwest*, vol. 1, *U.S. Geol. Surv. Prof. Pap.*, vol. 1560, edited by A. M. Rogers, T. J. Walsh, W. J. Kockelman, and G. R. Priest, pp. 257-283, 1996.
- Malone, S., R. S. Crosson, K. C. Creager, A. Qamar, G. C. Thomas, R. Ludwin, K. G. Troost, D. B. Booth, and R. A. Haugerud, Preliminary report on the $M_W = 6.8$ Nisqually, Washington earthquake of 28 February 2001, *Seismol. Res. Lett.*, 72, 353-362, 2001.
- Malone, S. D., and S. S. Bor, Attenuation patterns in the Pacific Northwest based on intensity data and the location of the 1872 North Cascades earthquake, *Bull. Seismol. Soc. Am.*, 69, 531-546, 1979.
- Massey, N. W. D., Metchosin igneous complex, southern Vancouver Island: Ophiolite stratigraphy developed in an emergent island setting, *Geology*, 14, 602-605, 1986.
- Miller, K. C., G. R. Keller, J. M. Gridley, J. H. Luetgert, W. D. Mooney, and H. Thybo, Crustal structure along the west flank of the Cascades, western Washington, *J. Geophys. Res.*, 102, 17,857-17,873, 1997.
- Molzer, P. C., U. S. ten Brink, M. A. Fisher, T. M. Brocher, K. C. Creager, and R. S. Crosson, Seismic structure of the Seattle fault, Seattle basin, and Kingston arch, Washington (abstract), *Eos Trans. AGU*, 80(46), F762, Fall Meet. Suppl., 1999.
- Nelson, A. R., S. K. Pezzopane, and R. C. Bucknam, Holocene surface faulting in the Seattle fault zone, Bainbridge Island, Washington (abstract), *Seismol. Res. Lett.*, 70, 233, 1999.
- Parsons, T., R. E. Wells, and M. A. Fisher, Three-dimensional velocity structure of Siletzia and other accreted terranes in the Cascadia forearc of Washington, *J. Geophys. Res.*, 104, 18,015-18,039, 1999.
- Pratt, T. L., S. Johnson, C. Potter, W. Stephenson, and C. Finn, Seismic reflection images beneath Puget Sound, western Washington state: The Puget Lowland thrust sheet hypothesis, *J. Geophys. Res.*, 102, 27,469-27,489, 1997.
- Ramachandran, K., Velocity structure of S.W. British Columbia, and N.W. Washington, from 3-D non-linear seismic tomography, Ph.D. thesis, 198 pp., Univ. of Victoria, Victoria, British Columbia, Canada, 2001.
- Schruben, R. A., R. E. Arndt, W. J. Bawiec, and R. A. Ambroziak, Geology of the coterminous United States at 1:2,500,000 scale: A digital representation of the 1974 P. B. King and H. M. Beikman map, *U.S. Geol. Surv.*, Denver, Colo., 1994.
- Schultz, A. P., and R. S. Crosson, Seismic velocity structure across the central Washington Cascade range from refraction interpretation with earthquake sources, *J. Geophys. Res.*, 101, 27,899-27,915, 1996.
- Sherrod, B. L., Late Holocene environments and earthquakes in southern Puget Sound, Ph.D. thesis, 159 pp., Univ. of Wash., 1998.
- Snively, P. D., and E. M. Baldwin, Siletz River volcanic series, northwestern Oregon, *Bull. Am. Assoc. Petrol. Geol.*, 32, 805-812, 1948.
- Snively, P. D., Jr., and R. E. Wells, Cenozoic evolution of the continental margin of Oregon and Washington, in *Assessing Earthquake Hazards and Reducing Risk in the Pacific Northwest*, vol. 1, edited by A. M. Rogers, T. J. Walsh, W. J. Kockelman, and G. R. Priest, *U.S. Geol. Surv. Prof. Pap.*, vol. 1560, pp. 161-182, 1996.
- Symons, N. P., Seismic velocity structure of the Puget Sound region from 3-D non-linear tomography, Ph.D. thesis, 168 pp., Univ. of Washington, Seattle, Wash., 1998.
- Symons, N. P., and R. S. Crosson, Seismic velocity structure of the Puget Sound region from 3-D non-linear tomography, *Geophys. Res. Lett.*, 24, 2593-2596, 1997.
- Tabor, R. W., Late Mesozoic and possible early Tertiary accretion in western Washington state—the Helena-Haystack melange and the Darrington-Devils Mountain fault zone, *Geol. Soc. Am. Bull.*, 106, 217-232, 1994.
- Tabor, R. W., and W. M. Cady, Geologic map of the Olympic Peninsula, Washington, *U.S. Geol. Surv. Misc. Invest. Ser.*, Map I-994, scale 1:125,000, 1978a.
- Tabor, R. W., and W. M. Cady, The structure of the Olympic Mountains, Washington—analysis of a subduction zone, *U.S. Geol. Surv. Prof. Pap.*, 1033, 38 pp., 1978b.
- Tabor, R. W., V. A. Frizzell Jr., D. B. Booth, R. B. Waitt, J. T. Whetten, and R. E. Zartman, Geologic map of the Skykomish River 30- by 60-minute quadrangle, Washington, *U.S. Geol. Surv. Misc. Invest. Ser.*, Map I-1963, scale 1:100,000, 1993.
- ten Brink, U. S., P. C. Molzer, M. A. Fisher, R. J. Blakely, R. S. Crosson, and K. C. Creager, Subsurface geometry and evolution of the Seattle fault zone and the Seattle basin, *Bull. Seismol. Soc. Am.*, 92, 1737-1753, 2002.

- Trehu, A. M., I. Asudeh, T. M. Brocher, J. H. Luetgert, W. D. Mooney, J. L. Nabelek, and Y. Nakamura, Crustal architecture of the Cascadia forearc, *Science*, 266, 237–243, 1994.
- Wang, K., Simplified analysis of horizontal stresses in a buttressed forearc sliver at an oblique subduction zone, *Geophys. Res. Lett.*, 23, 2021–2024, 1996.
- Wang, K., J. He, and E. E. Davis, Transform push, oblique subduction resistance, and intraplate stress of the Juan de Fuca plate, *J. Geophys. Res.*, 102, 661–674, 1997.
- Wells, R. E., D. C. Engebretson, P. D. Snively Jr., and R. S. Coe, Cenozoic plate motions and the volcano-tectonic evolution of western Oregon and Washington, *Tectonics*, 3, 275–294, 1984.
- Wells, R. E., C. S. Weaver, and R. J. Blakely, Fore-arc migration in Cascadia and its neotectonic significance, *Geology*, 26, 759–762, 1998.
- Yount, J. C., and H. D. Gower, Bedrock geologic map of the Seattle 30' by 60' quadrangle, Washington, *U.S. Geol. Surv. Open File Rep.*, 91-147, 37 pp., scale 1:100,000, 5 sheets, 1991.
-
- T. M. Brocher, U.S. Geological Survey, 345 Middlefield Road, MS-977, Menlo Park, CA 94025, USA.
- K. C. Creager, R. S. Crosson, G. Medema, and L. Preston, Department of Earth and Space Sciences, University of Washington, Box 351310, Seattle, WA 98195-1310, USA. (crosson@u.washington.edu)
- N. P. Symons, Sandia National Laboratories, Box 5800, MS-0750, Albuquerque, NM 87185-0750, USA.
- T. M. Van Wagoner, ChevronTexaco North America Upstream, 935 Gravier Street, New Orleans, LA 70112, USA. (thmv@chevrontexaco.com)